Experimental and Analytical Study of Mode II Interlaminar Failure of Bolted and Bonded Composite Structures

Phillip Gray

A thesis

submitted in partial fulfillment of the

requirements for the degree of

Master of Science in Aeronautics and Astronautics

University of Washington

2012

Committee:

Kuen Y. Lin

Mark Tuttle

Program Authorized to Offer Degree:

Department of Aeronautics and Astronautics

University of Washington

Abstract

Experimental and Analytical Study of Mode II Interlaminar Failure
of Bolted and Bonded Composite Structures

Phillip Gray

Chair of the Supervisory Committee:

Professor Kuen Y. Lin

Department of Aeronautics and Astronautics

The capability of a fastener to arrest and stabilize pure Mode II interlaminar failure in composite structures has been investigated both experimentally and analytically. A novel pure Mode II three-beam axially loaded specimen was designed specifically for the study. Test specimens were manufactured with $[(0/45/90/-45)_3]_S$ quasi-isotropic carbon fiber composite laminates for each beam. Teflon inserts were installed as initial cracks, and several variations of plies and bonding techniques were used at the crack interface. Testing showed that crack initiation loads depended on the plies at the crack interface and the bonding technique used. The fracture toughness of the bond in several configurations resulted in the crack initiation loads being higher that the load at which filled-hole tension failure of the laminates occurred; in such cases the full arrestment capability of the fasteners was not able to be captured, but post failure C-scans showed that the presence of a fastener did provide more crack arrestment than without a fastener. However, the testing of other specimens with lower fracture toughness of crack interface bonds displayed the capability of the fastener to arrest and stabilize a crack before filled-hole tension failure.

An analytical model and solution were developed to simulate crack growth in the three-beam specimen. The analytical solution was verified using FEM, and showed very good agreement of the results. The analytical model was used to determine the critical Mode II strain energy release rate, G_{IIC}, of each specimen configuration. Also, the analytical model was used to perform a series of parametric analysis of the three-beam specimen to study the effect that changing specimen parameters, such as laminate layup and thickness, had on the crack propagation behavior of the specimen. It was advised that the analytical model be used to aid in the design of alternate specimen configurations for further study.

TABLE OF CONTENTS

Page

LIST OF FIGURES

Page

LIST OF TABLES

Page

ACKNOWLEDGEMENTS

I would like to thank my advisor, Professor Kuen Y. Lin, for his guidance and support throughout my educational experience. I would also like to thank Chi Ho Cheung, who proved to be an invaluable colleague while working on this project, and Erik Bruun who helped with the project. I would also like to thank Professor Mark Tuttle and Bill Kuykendall for their support. Additional thanks go to Gerry Mabson, Marc Piehl, and Eric Cregger for their technical support. Finally, my sincerest thanks to my wife Natalie for her support throughout my education.

This thesis was jointly supported by The Boeing Company and the Federal Aviation Administration (FAA) through the AMTAS (Advanced Materials in Transport Aircraft Structures) at the University of Washington.

Chapter 1

INTRODUCTION

1.1 Introduction

Many types of fiber reinforced composite materials have been developed and used in a wide variety of structures since the 1960s. Composite materials have been used in aircraft structural applications because of their excellent strength and stiffness properties and light weight. Over the past few decades the applications and use of carbon fiber composite structures has been expanded from their use in secondary aircraft structures to their current use in primary aircraft structures.

The use of composites in primary aircraft structures has many desirable qualities. The anisotropy of composites allows for the strength and stiffness of structures to be directionally dependent; this is a great advantage for structures such as stringers, which mainly carry loads longitudinally. Also, composite structures reduce part counts and allow for large bonded surfaces to transfer loads between components, such as a fuselage stringer. An ideal structure could be engineered to be entirely bonded without the need of fasteners for assembly. But in actual aircraft structures, manufacturing defects, impact damage, fatigue, and geometric discontinuities can cause bonds to fail. Therefore there is a need for fasteners as disbond arrest mechanisms in the structures. Because a disbond can cause critical structural failure, it is important to understand the behavior of disbonding of structures and how a fastener interacts with the disbond. This thesis is an experimental and analytical study of the interaction of a fastener with a pure Mode II disbond in composite structures.

1.2 Objective

The objective of this thesis is to design and conduct an experiment to investigate the capability of a fastener to arrest and stabilize pure Mode II crack propagation in composite structures, and to develop a closed-form analytical solution to simulate the crack growth of the experimental design, and provide a parametric analysis tool.

1.3 Background

There has been recent research on fracture testing of bolted and bonded (hybrid) composite joints. A number of tests have been conducted on composite hybrid single lap joints. For example, Jen and Lin [1,2] performed tensile strength tests of several hybrid single lap configurations, varying stacking sequence, overlap length, fastener properties, rivets, and clamping force. The results did in fact produce disbonding of the joint, and subsequent loading of the fastener, which, depending on the configuration, continued to carry the joint load. An unavoidable result of a single lap configuration is that disbonding occurs as mixed-mode (Modes I and II) because of bending of the adherends from the asymmetry of the load path. Lee et al. [3] performed strength testing of composite hybrid double lap joints. A double lap joint has a symmetric load path. From the tests, images show failure occurred as disbonding from the single end of the joint and propagated to the fastener, where the load began to be transferred by the fastener. Although the load path is symmetric, there is a peeling force that develops at the end of the joint that causes mixed mode crack propagation. The review of single and double hybrid lap joints showed that crack propagation is initiated followed by loading of the fastener, but disbonding of the joints occur in mixed mode, which is undesirable for this study.

Currently there is no ASTM standard for pure Mode II interlaminar fracture. ASTM D6671 [4] involves interlaminar fracture testing of a three-point end notched flexure (ENF) specimen for measureing fracture toughness, but the disbonding of the specimen is mixed

mode and does not accommodate a fastener. Testing has been performed with three-point ENF flexural-type specimens that do result in pure Mode II fracture. For example, Todo et al. [5] performed a quasi-static three-point ENF test to measure the critical strain energy release rate (SERR), G_{IIC}, of composites. The tests successfully resulted in pure Mode II crack propagation of the composites. Carlsson et al. [6] conducted a study on the analysis and design of ENF specimens for Mode II testing. The study showed that deflection of the ENF must be limited in order to maintain linear behavior of the specimen. For materials with relatively high fracture toughness, greater loads are required to propagate a crack, therefore the thickness of the specimen must be increased to limit deflection. The addition of a fastener increases the effective fracture toughness as a crack grows, and the length available for crack growth is limited. The effect of this is that the length and thickness of the specimen becomes coupled with arrested crack growth, and the specimen becomes unreasonably long and thick to perform any testing. The ENF tests are specifically designed to provide G_{IIC} values of the material, not to perform crack arrestment tests. Therefore, the ENF configuration is undesirable for the current study.

Research has been conducted on the transfer of loads by fasteners from multi-row fastener joints. Tate and Rosenfeld [7] developed a solution for the load transferred by fasteners in symmetric butt joints by solving for the fastener compliance. The solution was derived for multi-fastener metallic symmetric butt joints. The total fastener compliance is given as the sum of four individual compliances as follows: fastener shear, fastener bending, fastener bearing, and plate bearing. It was stated that, based on the assumptions made, further testing of a variety of joint configurations would be necessary for the equation to be generally acceptable. More recently, Huth [8] developed an empirical expression for fastener compliance of multi-row single and double lap joints, based on empirical data. The solution for fastener compliance is valid for bolted metallic joints, riveted metallic joints, and bolted graphite/epoxy joints. Several experiments were conducted, which showed the analytical expression was able to accurately predict the fastener transfer loads. Huth claimed that his solution was a more accurate that previously existing expressions. It was important to have an expression for fastener compliance of multi-row fastened joints. Although the current study is for single fasteners, the load is not entirely transferred by the single fastener. The

load is transfer by both the fastener and the bond at the crack tip, which is analogous to a multi-fastener joint.

With disbond and delamination being common failure modes in composites, research has been conducted on determining the onset of these failure modes. A method that is commonly used for a wide variety of applications is the virtual crack closure technique [9] (VCCT). VCCT considers the force required to close a crack at a short distance from the crack tip. Based on this information the load at which a crack would propagate at the small distance is equal to the load required to close the crack. The method is very powerful, because it provides full strain energy release rate (SERR) mode decomposition for Modes I, II, and III, from relatively simple expressions. VCCT is very well suited for finite element modeling (FEM) because it relies on local information at the crack tip, for example the force between two nodes of adjacent elements. VCCT has been implemented in the commercial FEM code ABAQUS [10]. Although it is very powerful, VCCT is not desirable for the current study, because the local behavior at the crack tip must be resolved in addition to the global behavior. More recently Wang and Qiao [11] have developed closed-form expressions for the SERR Mode I and II decomposition of asymmetric and bi-material double cantilever beams (DCB), which are subject to combined axial and transverse loading conditions. The expressions take into account the rotation and shear deformation of the beams at the crack-tip. The total SERR is decomposed in Mode I and II in a global sense. The research concluded that the developed solution provided better agreement with finite element models than classical solutions. The solution does take into account the global behavior of a DCB, but for fracture analysis of more complex structures, the region of fracture must be treated independently as a DCB.

In general there is a lack of existing experimental work dealing with the ability of a fastener to arrest pure Mode II crack propagation. Pure Mode II test specimens do exist (ENF), but the main purpose of the tests is to obtain material data, G_{IIC}, and they do not accommodate a fastener or relatively large cracks. The existing solutions to predict the onset of fracture, although sophisticated and powerful, do not take directly into account the global

behavior of complex structures, such as structures containing fasteners, and the area of fracture must be treated independently. With this, there is a need to develop an interlaminar test specimen, which results in pure Mode II crack propagation that can accommodate a fastener to provide crack arrestment while allowing enough room for a crack to grow. Additionally there is a need for a simple expression that can predict the behavior of the specimen to use as an aid in design and analysis. This is the goal of this thesis.

Chapter 2

DESING OF PURE MODE II INTERLAMINAR FRACTURE SPECIMEN

2.1 Existing Pure Mode II Composite Interlaminar Facture Specimens

Currently, there is no ASTM standard for a pure Mode II composite interlaminar fracture specimen. ASTM-D6671 [4] deals with interlaminar fracture toughness, but uses a bending specimen that results in mixed mode (Mode I and II) fracture. Bending split-beam specimens are commonly used to measure the Mode II critical strain energy release rate, G_{IIC}; examples of these include but are not limited to: 3-point End Notched Flexture (ENF), 4-point ENF, and End Loaded Split (ELS), examples of these are shown in Figure 3.1. The benefit of using bending of a split-beam for Mode II crack propagation is the ability to keep the crack tip closed, which keeps G_I at zero. These types of specimens also result in stable crack propagation, which means that multiple measurements could be taken from a single coupon. However, the total deflection of the specimen is limited to maintain linear behavior, which results is a high thickness to length ratio, and the length available to allow crack propagation is relatively small.

Unfortunately, these bending specimens are specifically designed to only measure G_{IIC}. They are not suitable for crack arrestment tests and typically do not include a fastener either. The leading issue is that the length available for crack growth is very limited, because it is coupled with the size of the specimen. For a typical bending specimen, only a fraction of its full length can be used for crack propagation. There is not sufficient space for fastener installation to demonstrate the effectiveness of the fastener to arrest a crack. The only way to increase the available crack-growth area is to increase the specimen length, which requires increasing the specimen thickness to maintain linearity or bending failure. Also, as the effective G_{IIC} increases with the presence of a fastener, the amount of deflection required to obtain results increases; this can lead to bending failure before crack arrestment be tested.

The presence of the fastener also introduces a bending moment when loaded, which adds non-linearity and complexity to the simple split-beam system. The general lack of control of the test parameters means that these specimens are not suitable for this research.

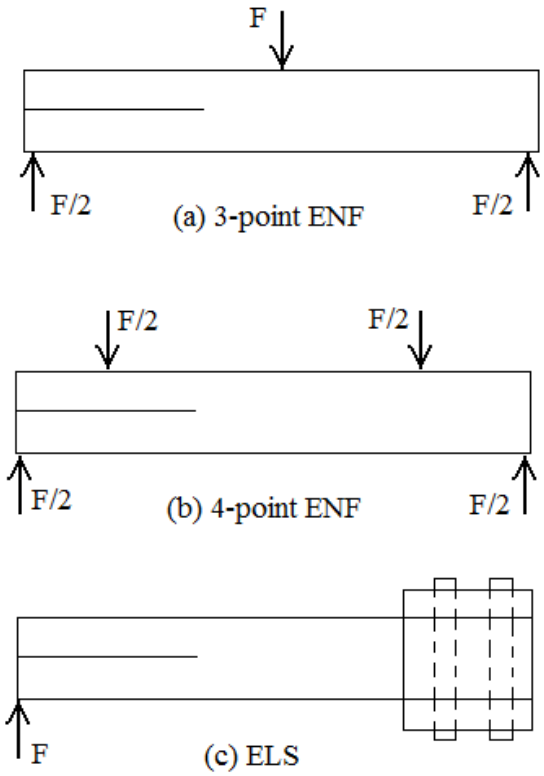

Figure 2.1: Examples of Flexure Mode II Disbond/Delamination Test Specimens

2.2 Proposed Three-Beam Axially Loaded Specimen

Because the flexural specimens are not desirable, two candidates for a novel Mode II crack arrestment specimen have been proposed, shown in Figure 2.2. One is a center-load specimen and the other is an outer-load specimen. The three-beam design ensures that load and deformation will be symmetric about the mid-plane, which eliminates coupling of out of plane bending and extension. The specimen can be lengthened as desired to provide ample space for crack propagation without the need to increase the thickness. This design provides freedom in the choice of different layup combinations; the layup is only limited by the need

to accommodate the fastener joint. Such specimen would be simple to manufacture and easy to test in any axial load frame.

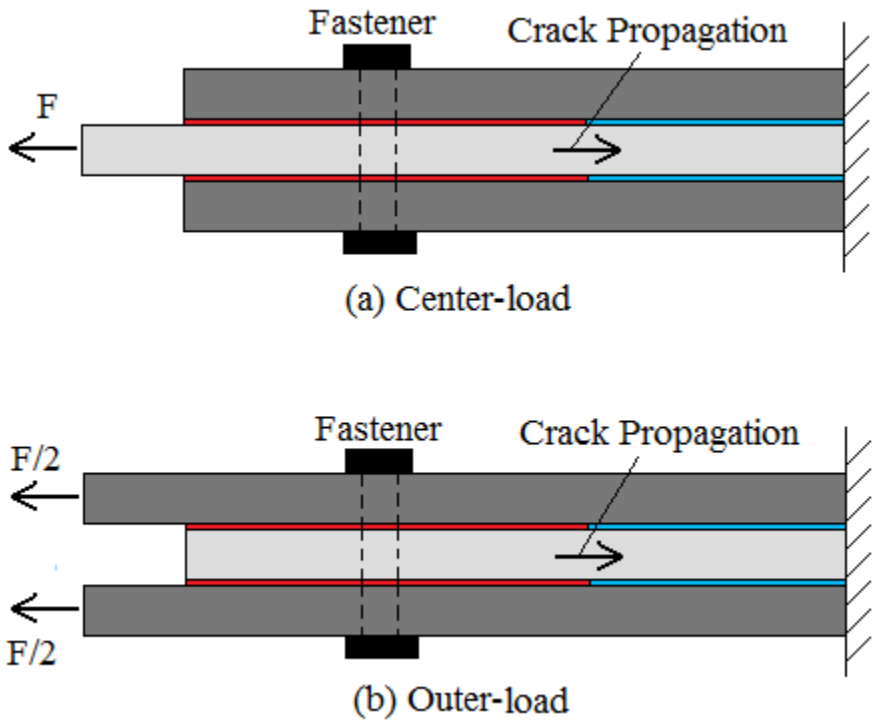

Figure 2.2: Proposed axial three-beam specimens

A finite element model (FEM) was constructed in ABAQUS to analyze the crack propagation characteristic of the candidate three-beam specimens. The model information is summarized in Table 2.1. Figure 2.3 shows the FEM in a non-deformed state and the deformed states for both center-load and outer-load configurations. The total length of the FEM is 12.5 in, and the thickness of each beam is 0.18 in. The initial crack extends to 4.25 in from the loaded end of the model (left end in Figure 2.3). The fastener is located at 4.5 in past the loaded end. This leaves 8.0 in for the cracks to propagate past the fastener to the fixed end. For the first run, the center beam is uniformly loaded in tension over the cross-section at the free end, for the second run the outer beams are uniformly loaded over the cross section at the free end. A fixed boundary condition is applied to all three beams at the

Table 2.1: FEM details

Parameter	**Value**
Lamina properties (AS4/3501-6)	
E_1	18.5 Msi
E_2	1.64 Msi
G_{12}	0.871 Msi
ν_{12}	0.3
Thickness	0.0075 in
Laminate Properties	
Center and outer laminate layups	$[(0/45/90/-45)_3]_S$
G_{IC}	1.5 lb-in/in^2
G_{IIC}	7.0 lb-in/in^2
Fastener Properties	
E	16.5 Msi
E_x	8.25 Msi
Diameter	0.25 in
Fastener joint stiffness	4.3 *10^5 lb/in
Fastener axial stiffness (2 springs)	2.15*10^5 lb/in
Element Properties	
Thickness	0.0075 in
Width	0.015 in
Element Type	4-node bi-linear plane strain quad (CPE4)
Fracture method	VCCT
Mixed mode fracture law	Reeder law (η=1.75)

(a) FEM no load

(b) FEM center-load

(c) FEM outer-load

Figure 2.3: FEM unloaded (a), FEM center-load (b), FEM outer-load (c)

opposite end. The fastener is modeled as three springs; one spring models clamping of the fastener, no pre-load is applied, the other two model the transverse stiffness of the fastener. Rigid elements are attached to the line of nodes at the location of the fastener and the springs are attached to the rigid element, which prevent excessive deformation that would otherwise occur if the spring were attached to single nodes. Crack propagation is modeled using VCCT; cracks propagate to the next node when the mixed mode fracture law (Reeder Law, η=1.75) is reached.

The results of the FEM are shown in Figure 2.4. The figure shows the amount of Mode I and Mode II SERR that cause crack propagation for a given crack length. It was expected that after the crack passed beyond the fastener, the Mode I component would be eliminated by the clamping effect of the fastener and crack propagation would become pure Mode II. This is not true for the center-load configuration; crack propagation is mixed-mode. As the crack tip passes the fastener location, the clamping effect diminishes and G_I increases as the crack grows. This is because as the load is transferred through shear from the center to outer laminates at the crack tip, a moment is induced to maintain equilibrium; this is an opening moment at the crack tip, and therefore results in a Mode I component. This means that a three-beam, center-loaded specimen fails to provide a pure Mode II crack propagation across its length.

For the outer-load configuration the results show that crack propagation is entirely Mode II on both sides of the fastener. This is because the load is transferred through shear from the outer laminates to the center laminate at the crack tip; in order to maintain equilibrium a bending moment is induced. This is a closing moment at the crack tip that forces Mode I crack propagation to zero. The outer-load configuration is pure Mode II, which is independent of the fastener clamping force, and results strictly from the closing moment induced at the crack tip. This can be seen in Figure 2.4, because crack propagation is pure Mode II before reaching the fastener.

Based of the FEM results it was determined that the thee-beam outer-load specimen would be used to conduct the crack arrestment experiments.

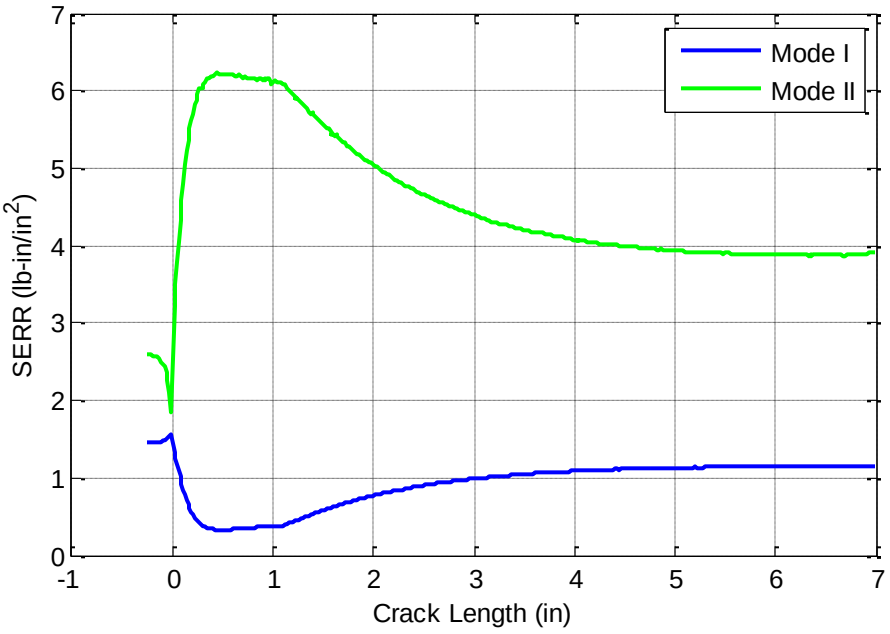

(a) SERR components for center-load

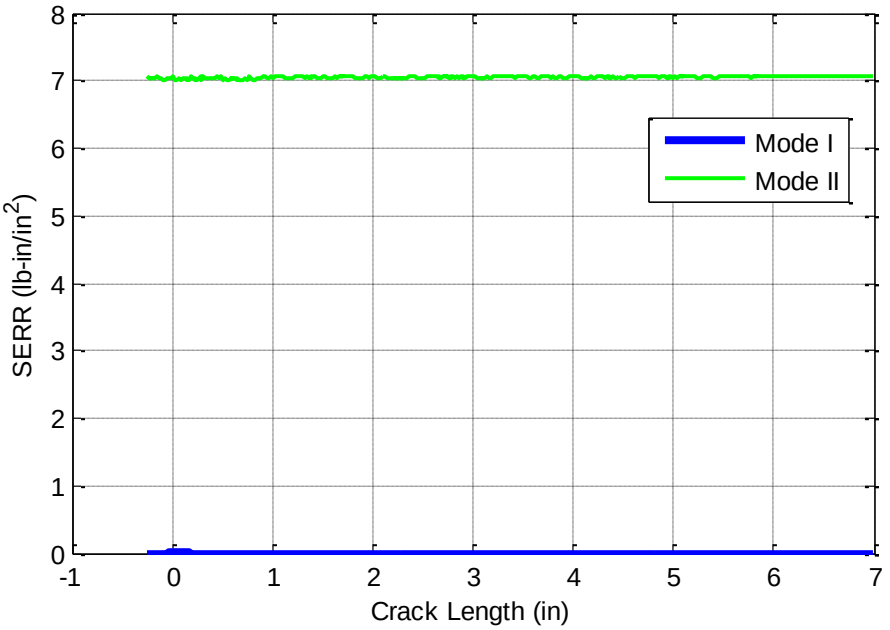

(b) SERR component for outer-load

Fig. 2.4 SERR versus crack length past fastener for center-load (a) and outer-load (b) configurations. The fastener is located at x = 0.

2.3 Design of the Three-Beam Specimen

The goal in designing the test specimen was to use laminates and a fastener that are representative of those used in actual structures. Because the goal of this experiment is to study the crack arrestment capability of fastener it was desired to design a specimen that would allow crack to propagate more easily. The design chosen was to use three 24-ply quasi-isotropic laminates bonded together, and a ¼" diameter titanium fastener. The exact dimension of the specimen and an image of an actual specimen are shown in Figure 2.5.

The specimen has a total length of 18.0 in. The specimen width is 1.25 in, which chosen as five times the diameter of the fastener. There are 3.0 in tabs at each end for clamping in to tensile test machine. There is a 1.0 in open gap at one end that provides the outer-loading that is required to achieve pure Mode II crack propagation. Next to the open gap at a length of 1.50 in are Teflon tabs that are inserted between the laminates to provide initial cracks. The fastener is placed 1.5 in from the crack tip, to avoid the stress concentrations at the hole affecting crack initiation.

During testing the specimen is loaded in tension and the cracks initiate from the implanted crack tip at each bond interface. The cracks then propagate un-arrested to the fastener, where the ability of the fastener to arrest and stabilize crack growth can be observed.

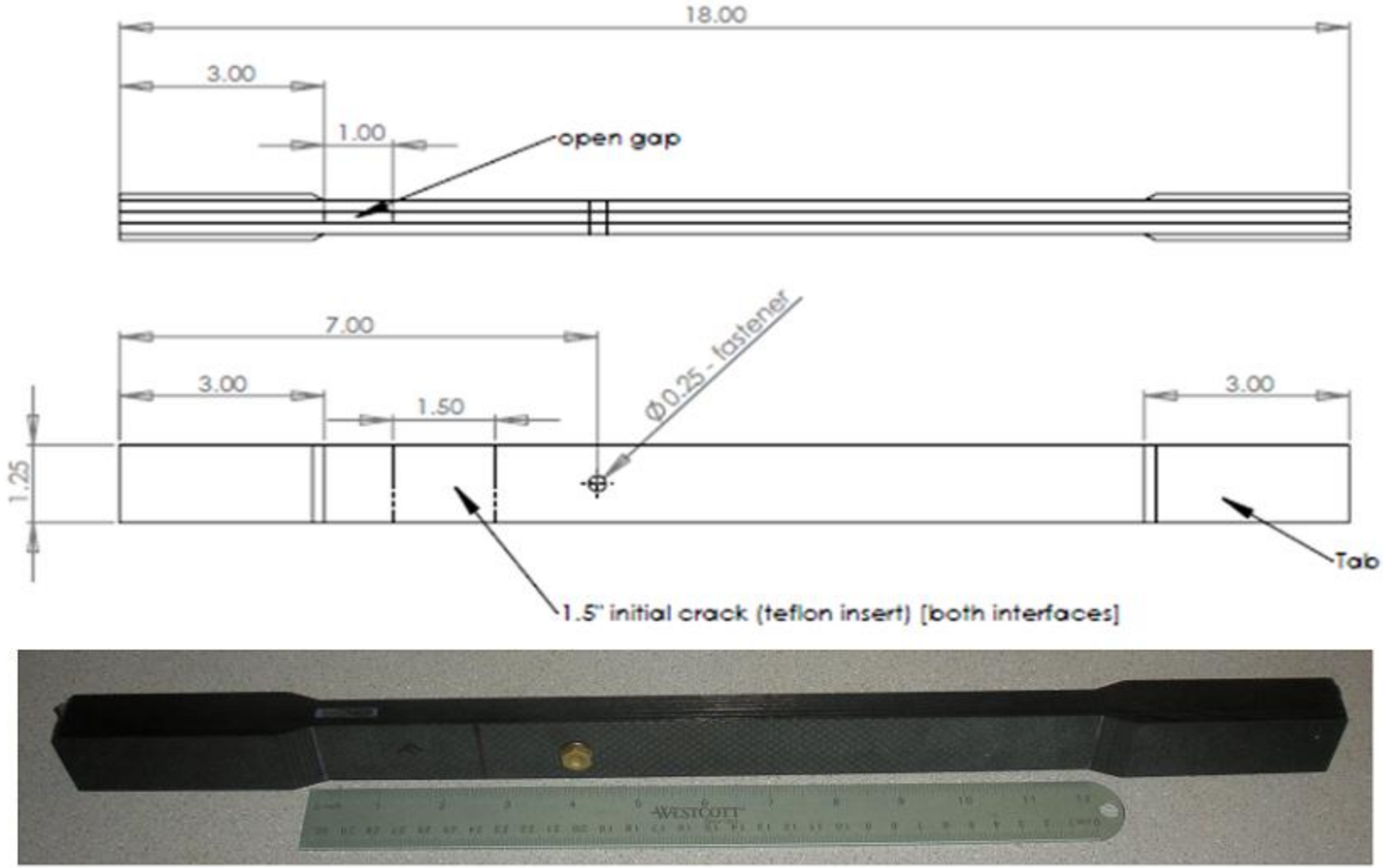

Figure 2.5: Three-beam specimen and dimensions

Chapter 3

EXPERIEMNTAL PROCEDURE

3.1 Test Matrix

Table 3.1 shows the test matrix for this experimental study. All specimens were manufactured by The Boeing Co., exact details of manufacturing and material data were not made available. A total of 18 specimens in 6 configurations were tested. The differences in specimen configurations are characterized by the bond type and plies at the crack interface. For all specimens, both outer and center laminates are 24-ply quasi-isotropic with layup $[(0/45/90/-45)_3]_S$. The outer plies of all outer laminates are [0/90] fabric, not 0, in order to prevent tearing when drilling the fastener holes. The plies at the crack interface vary as described in the test matrix. The material used is: T800H/3900-2.

The test matrix lists the Coupon ID, which is structured as follows: “Bond Type - Interface description – number”, for example: SB-0/90fab-2 is secondary bonded with [0/90] fabric plies at the bond interface number 2. Listed in the test matrix are bond type, interface plies, and fastener torque. A fastener torque that reads 0 in-lb (finger tight) was tightened until the fastener could not be rotated by hand.

Table 3.1: Test Matrix

Coupon ID	Bond Type	Interface Plies	Fastener Torque
SB-0/90fab-1	Secondary Bond	[0/90]/[0/90] fabric	40 in-lb
SB-0/90fab-2	Secondary Bond	[0/90]/[0/90] fabric	40 in-lb
SB-0/90fab-3	Secondary Bond	[0/90]/[0/90] fabric	40 in-lb
SB-0/90fab-4	Secondary Bond	[0/90]/[0/90] fabric	40 in-lb
SB-0/90fab-5	Secondary Bond	[0/90]/[0/90] fabric	40 in-lb
SB-0/90fab-6	Secondary Bond	[0/90]/[0/90] fabric	40 in-lb
SB-0/90fab-7	Secondary Bond	[0/90]/[0/90] fabric	40 in-lb
SB-0/90fab-8	Secondary Bond	[0/90]/[0/90] fabric	No Fastener
SB-0/0-1	Secondary Bond	0/0	0 in-lb (Finger Tight)
SB-0/0-2	Secondary Bond	0/0	0 in-lb (Finger Tight)
CC-0/0-1	Co-Cured	0/0	40 in-lb
CC-0/0-2	Co-Cured	0/0	40 in-lb
CC-0/0-3	Co-Cured	0/0	40 in-lb
CC-0/0-4	Co-Cured	0/0	40 in-lb
CC-±45-1	Co-Cured	+45/-45	0 in-lb (Finger Tight)
MB1-0/90fab-1	Modified Bond 1	[0/90]/[0/90] fabric	0 in-lb (Finger Tight)
MB1-0/90fab-2	Modified Bond 1	[0/90]/[0/90] fabric	40 in-lb
MB2-0/90fab-1	Modified Bond 2	[0/90]/[0/90] fabric	0 in-lb (Finger Tight)

3.2: Specimen Preparation

Each specimen had a strain gage installed on the outside of one of the outer laminates at 4.0 in from the fastener within the initial cracked region. The strain gages used are: Micro-Measurements EA-06-125AC-350. All stress values that are determined from the strain measurements are considered in this thesis to be "nominal stress". To determine the location of the crack, one side of the specimen was spray painted white and marked with black lines spaced at 0.125 in near the location of the fastener and spaced at 0.25 in away from the fastener. After strain gage installation and markings, the fastener was installed to the required torque. Figure 3.1 shows an example of the location of the strain gage and an image of the markings on the side of another specimen.

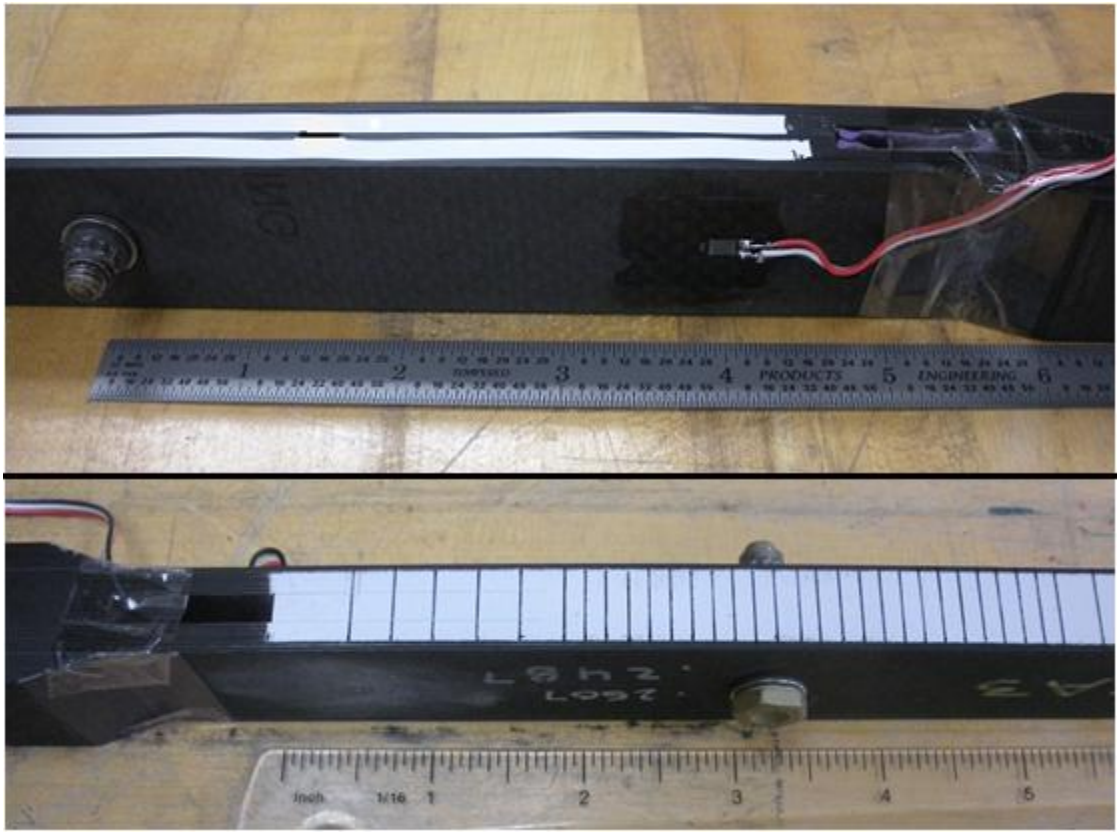

Figure 3.1: Strain gage location (top) and crack location markings (bottom)

3.3 Testing Procedure

All testing was conducted at the University of Washington Mechanical Engineering Department. After specimen preparations were completed, the specimens were loaded, individually, into a 55000 lb capacity Instron static load frame with mechanical grips. The strain gage was wired into a quarter-bridge Strain-Smart data acquisition system. The load frame was controlled on a computer by Instron software. The recorded data were total tensile load, load-frame head displacement, and strain. The loading of the specimens was displacement controlled at a rate of 0.20 in/minute. As the specimen load increased and the cracks began to propagate, the location of the crack tip was tracked visually by the markings on the side of the specimen. The load at which crack propagation occurred was read off of the computer that operated the Instron load frame. The test would continue until ultimate failure of the specimen occurred, or it was decided to stop testing. The load at the end of the test was recorded. Figure 3.2 shows a test specimen in the Instron load frame.

Figure 3.2: Specimen loaded in Instron load frame.

Chapter 4

MODE II CRACK PROPAGATION CHARACTERISTICS

4.1 Test Results of Secondary Bonded Specimens

The test results for all of the secondary bonded specimens are summarized in Table 4.1. For the secondary bonded specimens with [0/90] fabric plies at the interface, SB-0/90fab-1 through SB-0/90fab-8, crack initiation occurred at a nominal stress of 77.8-82.7 ksi. Nominal stress is defined as the stress in outer beams in the initially cracked region: $\sigma=P/(2A)$, where P is the total applied load, and A is the cross-sectional area of one outer beam. During testing, crack initiation was followed immediately by filled-hole or open-hole tension failure of the outer laminates at the location of the fastener hole. For the secondary bonded specimens with 0/0 plies at the interface, SB-0/0-1 and SB-0/0-2, crack initiation occurred at a nominal stress of 79.8-80.8 ksi. Crack initiation was followed immediately by filled-hole tension failure at the location of the fastener hole. For all of the secondary bonded specimens the crack initiation load was higher that the load at which the specimens failed in filled-hole or empty-hole tension failure.

Post-failure inspection of the secondary bonded specimens showed that for the specimens with the [0/90] fabric interface, SB-0/90fab-1 through SB-0/90fab-8, crack propagation was not cohesive; the cracks jumped a couple of plies into the outer laminates. The cracks were initiated at the bond interface, but jumped into the outer laminates and continued as a delamination. For all cases the cracks jumped into the outer laminates and propagated at a 90/45 interface. This is because the bonded fabric interface is stronger than the epoxy-lamina interface. The cracks propagated along the weakest ply interface. For the secondary bonded specimens with the 0/0 interface, SB-0/0-1 and SB-0/0-2, the crack did not jump into the outer laminates but remained cohesive as crack propagation occurred. Figure 4.1 shows a comparison of typical examples of both secondary bonded crack interfaces, 0/0

interface and [0/90] fabric interface. The figure also shows a typical example of the filled-hole and open-hole tension failure of the outer laminates.

Testing of the secondary bonded specimens showed that the crack initiation load was independent of the plies that were bonded at the interface. Although crack initiation loads were the same, the subsequent behavior of crack propagation was quite different; the 0/0 interface propagated cohesively, while the [0/90] fabric interface did not.

After testing, a C-scan was performed on two specimens, one with a fastener and one without a fastener, SB-0/90fab-7 and SB-0/90fab-8, respectively. The C-scan was conducted at the University of Washington Aeronautics and Astronautics department. The C-scan image is shown in Fig. 4.2. The upper image belongs to the specimen with a fastener and the lower belongs to the specimen without a fastener; red indicates good wave reflection (no disbond/delamination) and blue indicates the presence of discontinuity in the specimen (disbonded/delaminated). The C-scan images show that the presence of a fastener had a noticeable effect on crack propagation. For the specimen with a fastener, the crack front makes a “V” shape; the crack front wrapped around the fastener to 0.5 in at the edges, but the region directly behind the fastener remains fully intact. For the specimen without a fastener, the crack front is nearly straight across the specimen, at 0.75 in beyond the fastener location. The measurements are in inches and a scale is shown directly below each image scan; the fastener is at 0 in. Additional A-scan inspections of the rest of the specimens showed that the crack front shape is consistently similar to those shown in the C-scan image.

Table 4.1 Summary of results for secondary bonded specimens.

Specimen ID	Fastener Torque	Nominal Stress at Crack Initaiation	Failure Mode and Failure Stresss	Observed Crack Location at Failure
SB-0/90fab-1	40 in-lb	78.9 ksi	FHT (78.9 ksi)	NA
SB-0/90fab-2	40 in-lb	81.4 ksi	FHT (81.4 ksi	NA
SB-0/90fab-3	40 in-lb	82.2 ksi	FHT (82.2 ksi)	NA
SB-0/90fab-4	40 in-lb	81.8 ksi	FHT (81.8 ksi)	NA
SB-0/90fab-5	40 in-lb	77.8 ksi	FHT (77.8 ksi)	NA
SB-0/90fab-6	40 in-lb	82.7 ksi	FHT (82.7 ksi)	NA
SB-0/90fab-7	40 in-lb	80.5 ksi	FHT (80.5 ksi)	NA
SB-0/90fab-8	No Fastener	79.8 ksi	† OHT(79.8 ksi)	NA
SB-0/0-1	Finger Tight	79.8 ksi	FHT (79.8 ksi)	NA
SB-0/0-2	Finger Tight	80.9 ksi	FHT (80.9 ksi)	NA

FHT: Filled-hole tension failure

† OHT: Open-hole tension failure

NA: No crack observed before failure

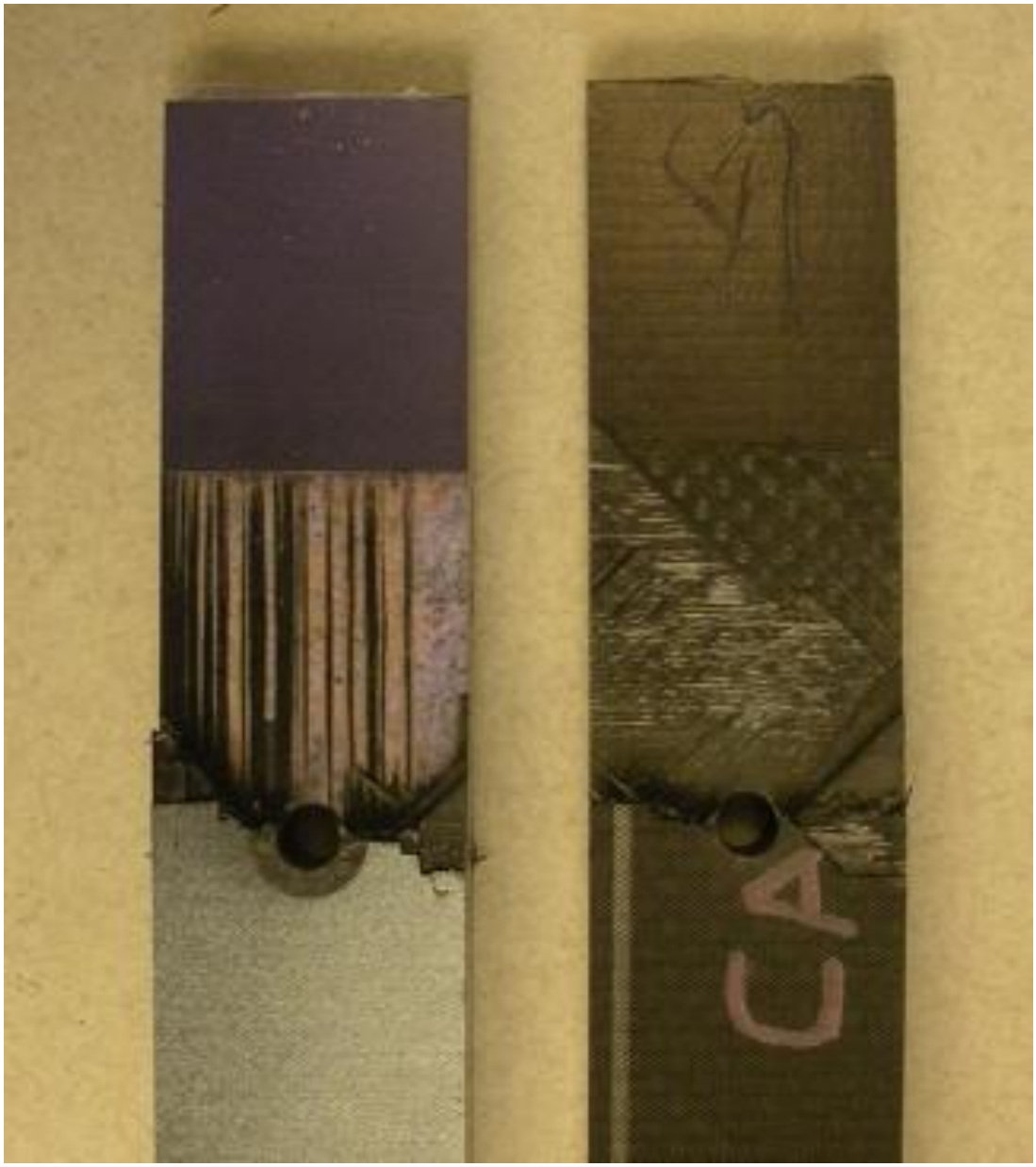

Fig. 4.1: Comparison of Secondary Bonded Specimen Crack Propagation (0/0 interface on left, [0/90] fabric interface on right). Both are filled-hole tension failure.

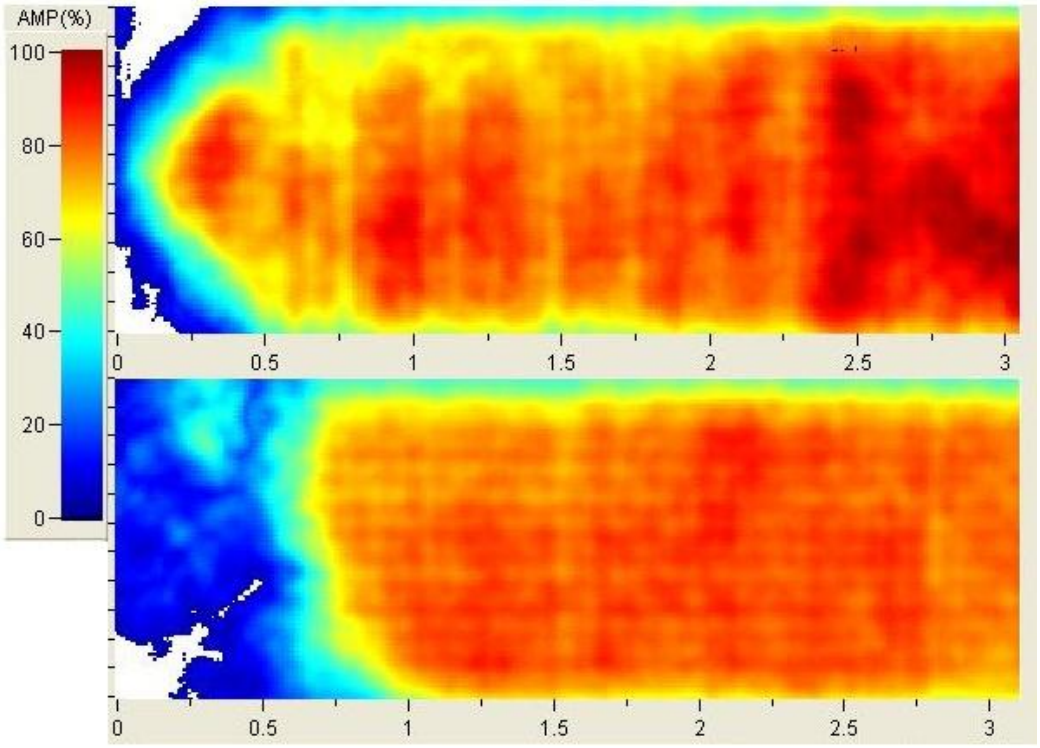

Fig. 4.2: C-Scan of secondary bonded specimens, with fastener installed (top) vs. no fastener installed (bottom)

4.2 Test Results of Co-Cured Specimens

The test results for all of the co-cured specimens are summarized in Table 4.2. For the co-cured specimens with 0/0 ply interface, CC-0/0-1 through CC-0/0-4, crack initiation occurred at a nominal stress of 45.8-54.0 ksi, while the initiation load for the co-cured specimen with the ±45 ply interface, CC-±45-1, was 60.2 ksi. The results showed that the crack propagation load was dependent on the plies at the crack interface. For the specimens with the 0/0 ply interface, the load at which filled-hole tension failure occurred was higher than the crack propagation load. For the specimen with the ±45° interface, the filled-hole tension failure load is approximately equal to the crack propagation load, and in this case failure of the specimen occurred almost immediately after crack initiation.

For the 0/0 ply interface specimens, crack propagation occurred cohesively; the crack remained entirely within the 0/0 ply interface. During testing, it was observed that crack

propagation from the Teflon insert to the fastener was not entirely unstable. The cracks propagated in small jumps of ~0.25 in, or appeared to grow. An increasing load was required to propagate the crack further. The tests showed that the cracks reached the region of the fastener at nominal stresses of ~10 ksi higher than at initiation. This was caused by a friction force created at the cracked interface from fastener clamping. The 0/0 interface specimens, CC-0/0-1 through CC-0/0-4, showed crack propagation past the fastener before the end of the tests. Performing an A-scan of the specimens shows that after testing: CC-0/0-1 has a straight crack front at 1.1 in past the fastener, and CC-0/0-2 has an angled, but straight, crack front at 1.1 in past on one edge and 0.5 in past on the other edge. The nominal stress at which CC-0/0-1 and CC-0/0-2 failed in filled holed tension failure is 67.6 and 66.0 ksi, respectively. The two specimens CC-0/0-3 and CC-0/0-4 were not tested to failure, and showed a V-shape crack front, where the crack location at the edges was 0.5 in past the fastener and the area directly behind the fastener was still intact. The nominal stress at which the tests were stopped for CC-0/0-3 and CC-0/0-4 were 65.6 and 65.1 ksi, respectively.

For the co-bonded ±45 interface specimen, CC-±45-1, the crack initiated within the implanted crack interface, but then propagated non-cohesively; the cracks jumped a couple of plies into the outer laminates and propagated within a 90/45 interface. This suggests that the implanted crack interface ply combination, ±45, is stronger than others within the laminate. The cracks propagated within the weakest interface of the laminates. The filled hole tension failure load of the ±45 interface specimen was less than the failure load of the co-cured 0/0 interface specimens. The reason for this is the jumping of the crack into the outer laminate; when the crack jumps into the outer laminates the cross-sectional area decreases, and therefore the failure actual stress at the location of the hole is higher than the nominal stess. An A-scan inspection of the ±45 interface specimen shows a straight crack front at 1.0 in past the fastener.

A comparison of both types of co-cured specimens is shown in Fig. 4.3.Testing of the co-cured specimens shows that a fastener has the ability to arrest crack propagation. The tests showed that with the presence of a fastener the crack was stabilized in the region of the

fastener and remained there until filled-hole tension failure of the specimen. Also, the relative strengths of different ply interface combinations were discovered. The 0/0 interface was weaker than the ±45 interface. And the 90/45 interface was also weaker than the ±45 interface.

Table 4.2 Summary of results for co-cured specimens.

Specimen ID	**Fastener Torque**	**Nominal Stress at Crack Initiation**	**Failure Mode and Failure Stress**	**Observed Crack Location at Failure**
CC-0/0-1	40 in-lb	45.8 ksi	FHT (67.6 ksi)	0.5 in past Fastener
CC-0/0-2	40 in-lb	43.1 ksi	FHT (66.0 ksi)	0.5 in past Fastener
CC-0/0-3	40 in-lb	47.1 ksi	Stopped before failure	0.5 in past Fastener
CC-0/0-4	40 in-lb	54.0 ksi	Stopped before failure	0.5 in past Fastener
CC-±45-1	Finger Tight	62.0 ksi	FHT (61.8 ksi)	NA

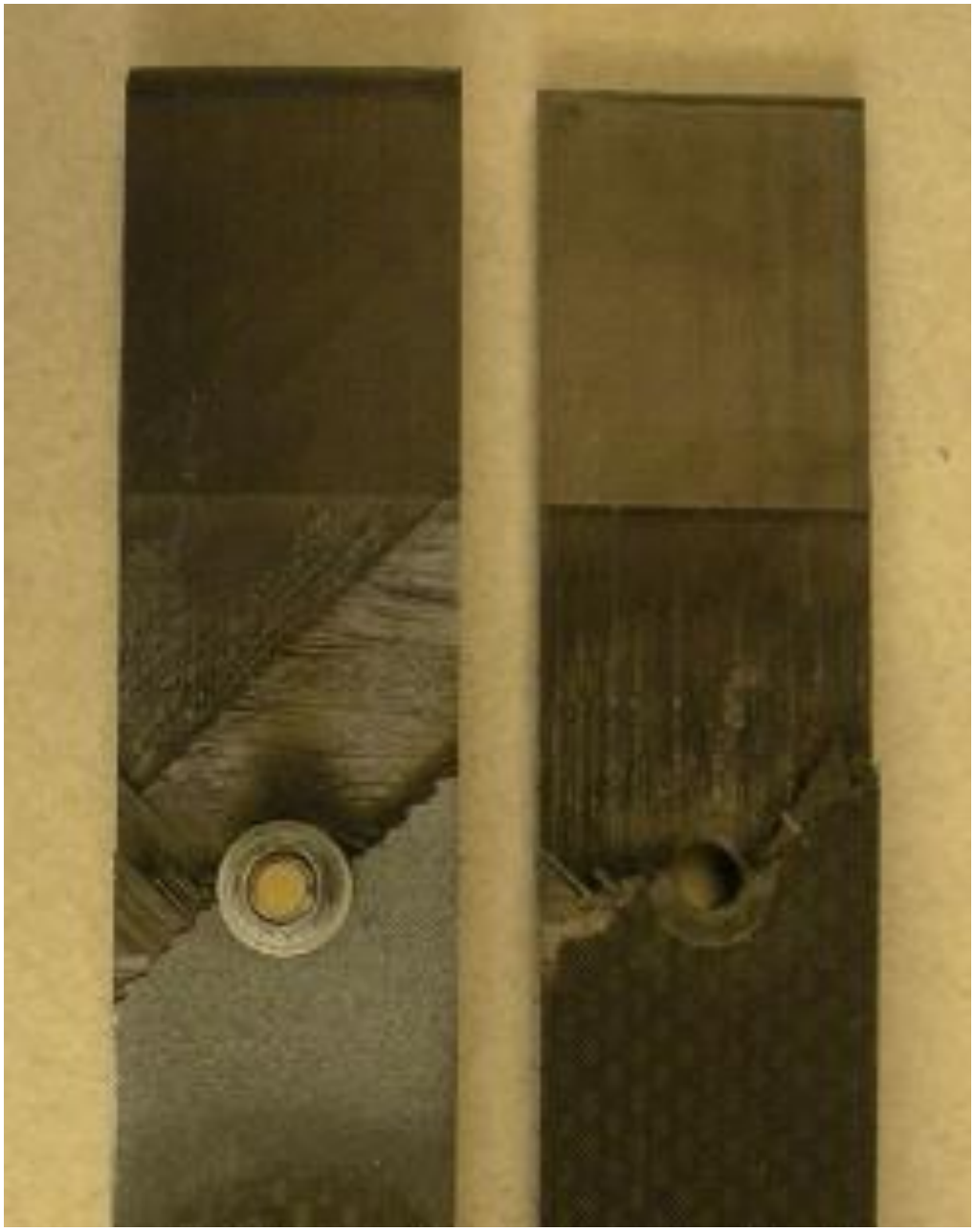

Fig. 4.3: Comparison of co-cured Specimen Crack Propagation (±45 interface on left, 0/0 interface on right). Both are filled-hole tension failure.

4.3 Test Results of Modified Bond Specimens

The test results for all of the modified-bond specimens are summarized in Table 4.2. The nominal stress at crack initiation for the modified-bond-1 specimens, MB1-0/90fab-1 and MB1-0/90fab-2, were 70.0 ksi and 68.4 ksi, respectively, while the filled-hole tension failure stresses were 65.6 and 68.7, respectively. Crack initiation and propagation occurred cohesively. For MB1-0/90fab-1 and MB1-0/90fab-2 specimens the cracks propagated unstably to the fastener and well beyond before being arrested completely. Each crack interface for each specimen reached a different length; crack propagation was not symmetric. For specimen MB1-0/90fab-1 the crack reached 3.5 in at one interface and 5.0 in at the other. For specimen MB1-0/90fab-2 the crack reached 4.75 in at one interface and 6.125 in at the other. After such a large crack propagation the load applied by the Instron load frame relaxed and decreased. The load then reached the filled-hole tension failure load and the specimens failed.

Testing of the modified-bond-1 specimens, MB1-0/90fab-1 and MB1-0/90fab-2, showed that the fastener did arrest unstable crack propagation for both cases. Another result is that the distance that the crack traveled past the fastener was related to the fastener torque. Specimen MB1-0/90fab-1 had a fastener torque of 40 in-lbs while specminen MB1-0/90fab-2 had a fastner torque of 0 in-lbs (finger tight); cracks propagated further on MB1-0/90fab-1 than on MB1-0/90fab-2.

The crack initiation load for the modified-bond-2 specimen, MB2-0/90fab-1, was 93.8 ksi, which was significantly higher than any other specimen tested. Immediately after crack initiation the specimen, MB2-0/90fab-1, failed in filled-hole tension failure. This is because the crack propagation load was significantly higher that the filled-hole failure load of the specimen. Figure 4.4 shows a typical modified-bond specimen after failure, all were nearly identical.

Table 4.3 Summary of results for modified-bond specimens.

Specimen ID	Fastener Torque	Nominal Stress at Crack Initaiation	Failure Mode and Failure Stress	Observed Crack Location at Failure
MB1-0/90fab-1	40 in-lb	70.0 ksi	FHT 65.6 ksi)	3.5-5.0 in past fastener
MB1-0/90fab-2	Finger Tight	68.4 ksi	FHT (68.7 ksi)	4.75-6.125 in past fastener
MB2-0/90fab-1	Finger Tight	93.8 ksi	FHT (93.8 ksi)	NA

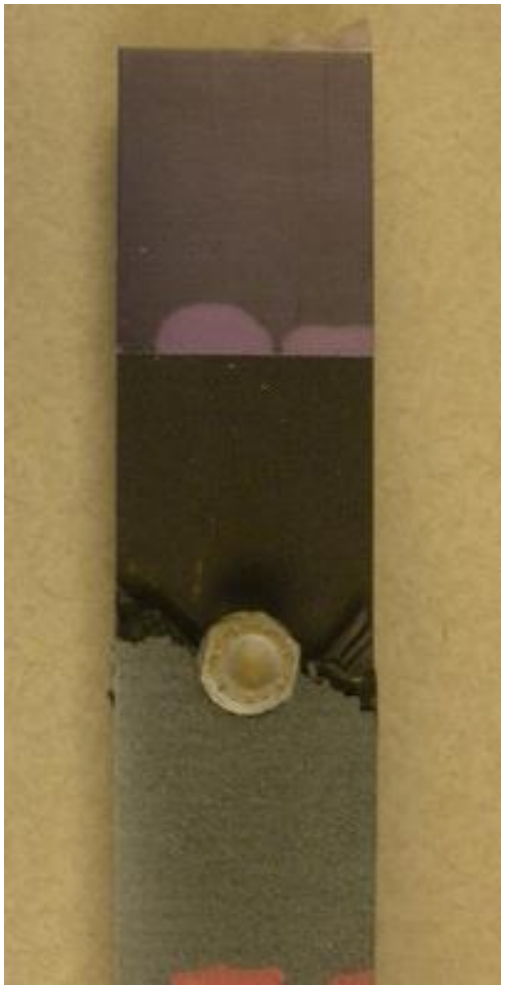

Figure 4.4: Typical modified-bond specimen

4.5 Measured Laminate Properties

The effective laminate modulus of elasticity in the x-direciton, E_x, was determined for each specimen configuration from measured load and strain data. Figure 4.5 shows a comparison of the typical plots for nominal stress versus measured strain for each configuration that was tested. The values of E_x were determined from Equation 4.1 and averaged over the linear range of the stress-strain curve. The nominal stress was calculated from the measured load-frame force divided by the nominal cross-section area. Strain was measured by strain gages. Table 4.4 summarizes measured E_x for all configurations.

$$E_x = \frac{\sigma_x}{\varepsilon_{x\,measured}} \tag{4.1}$$

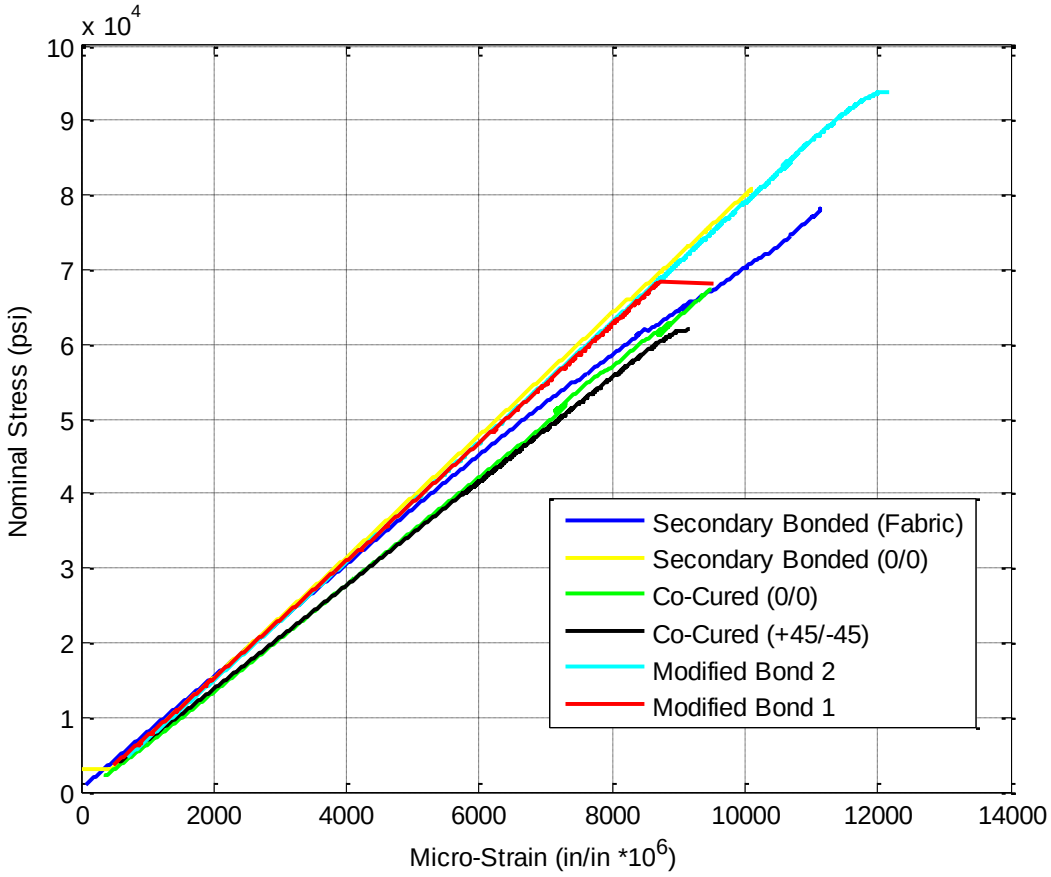

Figure 4.5: Typical plots for nominal stress versus measured strain

Table 4.4: Summary of Ex for all specimen configurations

Specimen Configuration	**Measured Ex**
Secondary bonded [0/90] fabric interface	7.44 Msi
Secondary bonded 0/0 interface	7.43 Msi
Co-Cured 0/0 interface	6.88 Msi
Co-Cured ±45 interface	6.92 Msi
Modified Bond 1	7.72 Msi
Modified Bond 2	7.82 Msi

From the strain measurements the filled-hole tensile failure strain of the outer laminates was averaged, for the laminates that failed in this manner. The average filled-hole tension failure strain, $\varepsilon_{\text{FHT avg}}$, was determined to be:

$$\varepsilon_{FHT\ avg} = 9460\ \mu\ in/in$$

Chapter 5

ANALYTICAL STUDY

5.1 Analytical Model Description

Figure 5.1 shows the full analytical model of the three-beam specimen. The origin of the model is located at the center of the fastener. The total load, P, is divided equally to the outer laminates in the free region at $x = -L_2$; for the free region: $x \in [-L_2, 0]$. The crack-tip is located at $x = a$; for the cracked region: $x \in [0, a]$. The specimen is fixed at $x = L_1$, at the end of the intact region; for the intact region: $x \in [a, L_1]$.

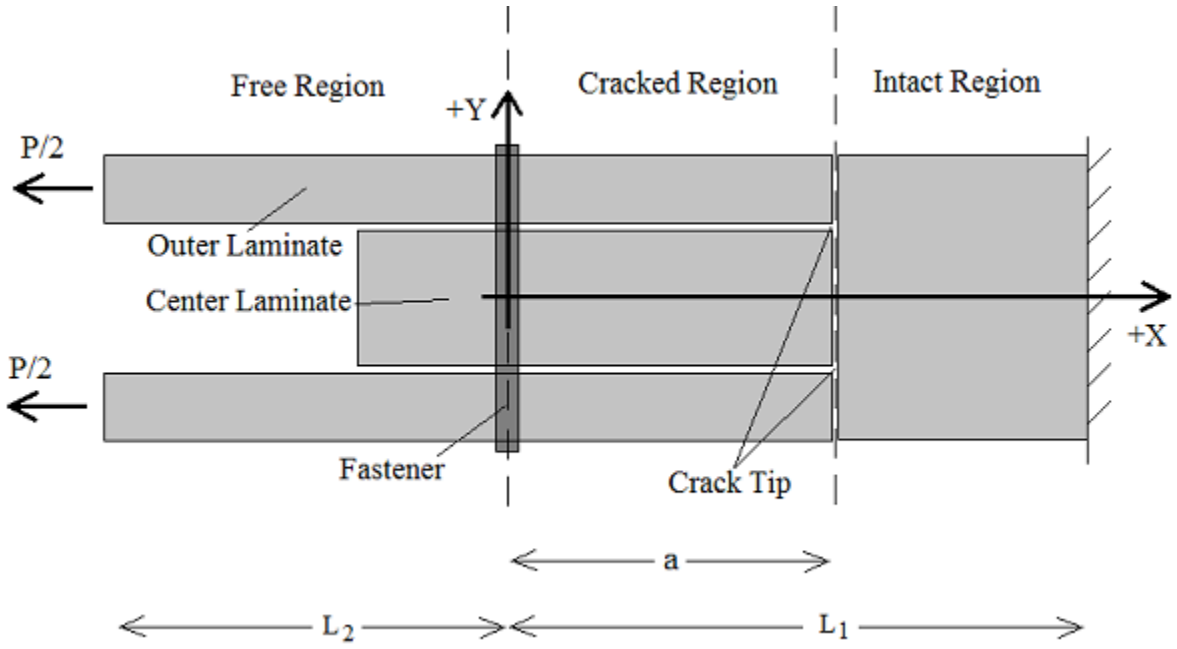

Figure 5.1: Full analytical model of three-beam specimen

The analytical model is simplified to an idealized model that replaces beams and the fastener with springs. In doing so the curvatures of the beams are assumed to be zero, the stress/strain distribution at the hole is ignored, and SERR mode decomposition is not considered. Friction within the crack interface is neglected. The idealized model is further simplified into the reduced-idealized model. This is done by considering the symmetry of the model about the x-axis. Figure 5.2 shows the full-idealized and the reduced-idealized analytical models.

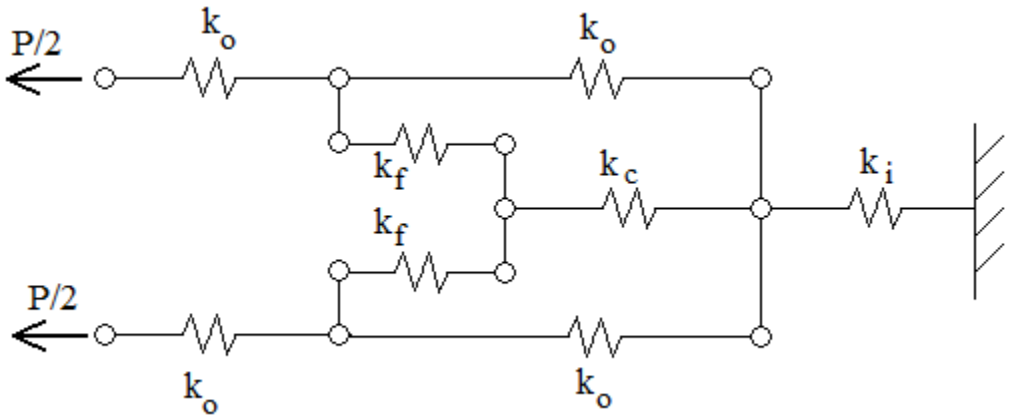

(a) Full idealized model

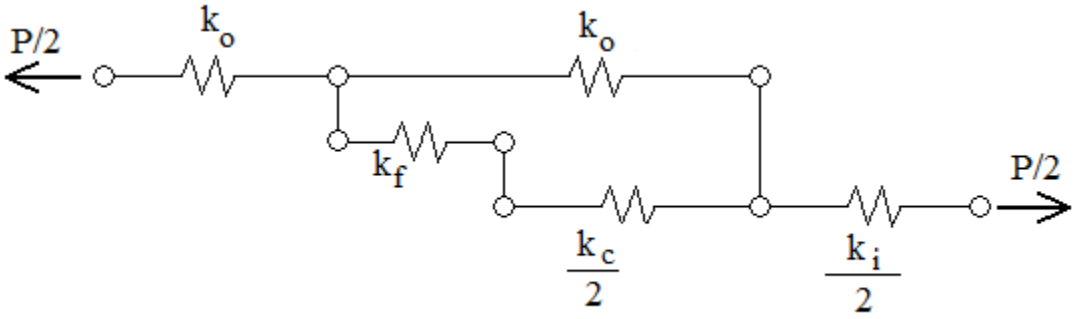

(b) Reduced idealized model

Figure 5.2: Full-idealized (a) and reduced-idealized (b) analytical models

5.2 Derivation of Closed Form Analytical Solution

In this section a closed from solution is derived that solves for the load at which cracks propagate, P_C, for an arbitrary crack length, a, as a function of laminate and fastener properties. For the derivation, first the fastener compliance, C_f, is determined, then the load transferred by the fastener, P_f, is solved, lastly the solution to P_C is derived.

5.2.1 Fastener Compliance

The fastener compliance, C_f, is determeind as described in [7]. From compliance, the stiffness is simply obtained from Eq. 5.1

$$k_f = \frac{1}{C_f} \tag{5.1}$$

The total fastener compliance is determined by considering the sum of the individual effects of fastener shearing, C_{fs}, fastener bending, C_{fb}, fastener bearing, C_{fbr}, and plate bearing, C_{pbr}, during the fastener load transfer. Equations 5.2 – 5.5 show the expressions for C_{fs}, C_{fb}, C_{fbr}, and C_{pbr}, respectively.

$$C_{fs} = \frac{2t_o + t_c}{3G_f A_f} \tag{5.2}$$

$$C_{fb} = \frac{8t_o^3 + 16t_o^2 t_c + 8t_o t_c^2 + t_c^3}{192E_f I_f} \tag{5.3}$$

$$C_{fbr} = \frac{2t_o + t_c}{t_o t_c E_f} \tag{5.4}$$

$$C_{pbr} = \frac{1}{t_o E_{x_o}} + \frac{2}{t_c E_{x_c}} \tag{5.5}$$

The total fastener compliance C_f is the sum of the four individual compliance components, as shown in Equation 5.6

$$C_f = C_{fs} + C_{fb} + C_{fbr} + C_{pbr} \tag{5.6}$$

Substituting Equations 5.2-5.5 into Equation 5.6 results in the full expression for the fastener compliance, shown in Equation 5.7. It can be seen that the fastener compliance is a function of geometric and material properties of the fastener, outer laminate, and center laminate.

$$C_f = \frac{2t_o + t_c}{3G_f A_f} + \frac{8t_o^3 + 16t_o^2 t_c + 8t_o t_c^2 + t_c^3}{192E_f I_f} + \frac{2t_o + t_c}{t_o t_c E_f} + \frac{1}{t_o E_{x_o}} + \frac{2}{t_c E_{x_c}} \tag{5.77}$$

5.2.2 Fastener Transfer Load

For the solution to the fastener transfer load, P_f, refer to the reduced analytical model that is shown in Figure 5.2. The first step is to solve for the equivalent stiffness of the center laminate and fastener, $k_{eq\ cf}$, and the equivalent stiffness of the outer laminate, center laminate, and fastener, $k_{eq\ ocf}$ as shown in Equations 5.8 and 5.9, respectively.

$$k_{eq\ cf} = \left[\frac{1}{k_{cc}} + \frac{1}{k_f}\right]^{-1} \tag{5.8}$$

$$k_{eq\ ocf} = k_{oc} + \left[\frac{1}{k_{cc}} + \frac{1}{k_f}\right]^{-1} \tag{5.9}$$

Next, Hooke's Law, for a spring, is used to solve for the displacement, x, of the equivalent spring due to the applied load, P/2. This is shown in Equation 5.10.

$$x = \frac{P/2}{k_{eq\ ocf}} \tag{5.10}$$

The fastener transfer load, P_f, can be determined by substituting Equations 5.8-5.10 into the expression for Hooke's Law, for a spring, as shown in Equation 5.11.

$$P_f = k_{eq\ cf} x = \frac{\left[\frac{1}{k_{cc}} + \frac{1}{k_f}\right]^{-1}}{k_{oc} + \left[\frac{1}{k_{cc}} + \frac{1}{k_f}\right]^{-1}} P/2 \tag{5.11}$$

5.2.3 Analytical Solution of Reduced Idealized Model

The analytical solution is derived directly from the definition of the strain energy release rate, G, as shown in Equation 5.12.

$$G = \frac{\partial U_{total}}{\partial a} \tag{5.12}$$

Where U_{total} is the total energy of the reduced idealized model, and is determined from the summation of the energies of the individual components that make up the model. Because each component of the model is analyzed as a spring, the energy of each component can be solved from the definition of the potential energy of a linear spring with a constant applied load, as described in Equation 5.13.

$$U_{spring} = \frac{1}{2} k P^2 \tag{5.13}$$

The potential energy of each component: outer laminate free, outer laminate cracked, center laminate cracked, intact laminates, and fastener are defined in Equations 5.14-5.18 respectively.

$$U_{of} = \frac{1}{2} k_o (P/2)^2 \tag{5.14}$$

$$U_{oc} = \frac{1}{2} k_0 \left(P/2 - P_f\right)^2 \tag{5.15}$$

$$U_{cc} = \frac{1}{2} k_c \left(P_f\right)^2 \tag{5.16}$$

$$U_i = \frac{1}{2} k_i (P/2)^2 \tag{5.17}$$

$$U_f = \frac{1}{2} k_f \left(P_f\right)^2 \tag{5.18}$$

The total potential energy of the system is the sum of the potential energies of each component defined in Equation 5.19.

$$U_{total} = U_{of} + U_{oc} + U_{cc} + U_i + U_f \tag{5.19}$$

As can be seen in the equations above, it is necessary to determine the stiffness, k, of each laminate component. The stiffnesses k_o, k_c, and k_i can be easily determined from the stiffness expression for a bar or truss member; the stiffness for each are shown in Equations 5.20-5.22, respectively.

$$k_o = \frac{E_{x_o} A_o}{a} \tag{5.20}$$

$$k_c = \frac{E_{x_c} A_c}{a} \tag{5.21}$$

$$k_i = \frac{E_{x_i} A_i}{L_1 - a} \tag{5.22}$$

Substituting the stiffness expressions, Equations 5.20-5.22, into the corresponding energy expressions, Equations 5.14-5.8, and summing the energy expressions, Equation 5.19, and taking the derivative of the total energy with respect to the crack length a, Equation 5.12, results in an expression for the Mode II SERR, G_{II}, as shown in Equation 5.23.

$$G_{II} = P^2 \left[\frac{-2\left(aA_cE_c + 2aA_oE_o + A_cA_oC_fE_cE_o\right)^2}{8A_i\left(aA_cE_c + 2aA_oE_o + A_cA_oC_fE_cE_o\right)^2 E_i} + \cdots \right.$$

$$\left. \cdots + \frac{A_i(2a^2A_cE_c + A_o\left(2a + A_cC_fE_c\right)^2 E_o)E_i}{8A_i\left(aA_cE_c + 2aA_oE_o + A_cA_oC_fE_cE_o\right)^2 E_i} \right] \tag{5.23}$$

Substituting the critical Mode II SERR, G_{IIC}, into Equation 23 and solving for P gives an expression for the critical load, P_C, at which crack propagation will occur in the three-beam model with an arbitrary crack length, a. Equation 5.24 shows this final expression.

$$P_C = \sqrt{G_{IIc}}\left[\frac{-2\left(aA_cE_c + 2aA_oE_o + A_cA_oC_fE_cE_o\right)^2}{8A_i\left(aA_cE_c + 2aA_oE_o + A_cA_oC_fE_cE_o\right)^2E_i} + \cdots\right.$$

$$\left. \cdots + \frac{A_i(2a^2A_cE_c + A_o\left(2a + A_cC_fE_c\right)^2E_o)E_i}{8A_i\left(aA_cE_c + 2aA_oE_o + A_cA_oC_fE_cE_o\right)^2E_i}\right]^{-\frac{1}{2}} \tag{5.24}$$

From Equation 5.24 the critical nominal stress, σ_C, is simply obtained by dividing P_C by the cross-sectional area of the two outer laminates, as shown in Equation 5.25.

$$\sigma_C = \frac{P_C}{2A_o} \tag{5.25}$$

The expressions in Equations 5.24 and 5.25 can be used to perform analytical crack propagation simulations for a wide variety of specimen geometries, laminate properties, critical SERR values, and fastener properties.

5.3 Verification of the Analytical Solution by FEM

The analytical solution was verified by using the finite element model that was previously described in section 2.2 for various G_{IIC} values. The lamina properties and fastener properties that were used in the finite element model are listed in Table 5.1; these are the same properties that are used in the analytical model.

Table 5.1: Lamina and fastener properties for FEM validation of the analytical model

Lamina Properties (AS4/3501-6)	
Lamina Property	**Property Value**
E_1	18.5 msi
E_2	1.64 msi
ν_{12}	0.3
G_{12}	0.871 msi
t	0.0075 in
G_{IC}	1.5 in-lb/in^2
G_{IIC}	7.0, 14.0, 20.0 in-lb/in^2
Fastener Properties (Titanium)	
Fastener Property	**Property Value**
E	16.5 msi
d	0.25 in
E_x	7.42 msi
G (shear modulus)	6.38 msi
C	$4.64*10^{-6}$

The layup used for both the outer laminates and center laminate, for both FEM and analytical model, is a 24-ply symmetric quasi-isotropic laminate.

Outer and center laminate layup: $[(0/4590/-45)_3]_S$.

Using classical lamination theory for the laminate described above the laminate A-matrix is as follows.

$$A = \begin{bmatrix} 1.471 & 0.445 & 0 \\ 0.445 & 1.471 & 0 \\ 0 & 0 & 0.513 \end{bmatrix} * 10^6 \ (psi * in)$$

From the A matrix, the effective in-plane laminate properties (E_x, E_y, G_{xy}, ν_{xy}, and ν_{yx}) were determined and are summarized in Table 5.2

Table 5.2: Effective in-plane laminate properties for $[(0/45/90/-45)_3]_S$.

In-plane Property	**Property Value**
E_x	7.424 Msi
E_y	7.424 Msi
G_{xy}	2.850 Msi
ν_{xy}	0.303
ν_{yx}	0.303

The analytical solution was run in Matlab. The curves are produces by solving for P_C at a given crack length, a, then allowing the crack length to increase by a small amount (simulation of growing crack) and solving for the new load, P_C, for which the crack propagates again. Figure 5.3 shows the comparison of the analytical model and finite element model for critical SERR values of 7.0, 14.0, and 20.0 in-lb/in^2. In the plot, the crack starts at x = -0.25 in, which is where unstable crack growth occurs, characterized by a horizontal slope. Cracks reach the fastener at x = 0 and are stabilized. A more positive slope indicates greater crack stability. The crack growth simulation is taken to 5.0 in past the fastener. The FEM was run using plane-strain elements, while the analytical model was formulated using a plane-stress approach. The analytical model was modified, as described in Equation 5.26, to convert it from plane-stress to plane-strain.

$$E_{x\ plane-strain} = \frac{E_{x\ plane-stress}}{\left(1 - \nu_{xy}\nu_{yx}\right)} \tag{5.26}$$

In Figure 5.3 the analytical model and FEM agree very well. For the simulations, no failure modes other than crack propagation are considered. The graph shows the applied nominal stress (y-axis) versus crack length (x-axis). A steeper curve indicates more stable crack growth, and a horizontal curve indicates unstable crack growth. The slopes of the curves are very close, but the FEM curves are slightly less steep. The reason for this is the FEM used two-dimensional elements, while the analytical model is one-dimensional; this allows shear deformation of the FEM near the crack tip which slightly relaxes the load applied to the crack tip.

Some important notes on the FEM results are as follows. The portion of the FEM plots from x ϵ [-0.25in, 0.5in] that curve up then go horizontal are a bi-product of the FEM numerical solver, and should actually follow a continuous path similar to the analytical model. For the case of G_{IIC} = 20 in-lb/in^2, the short horizontal jump was caused by unsymmetrical crack propagation, where one crack jumped ahead of the other, then both continued in unsymmetrical propagation.

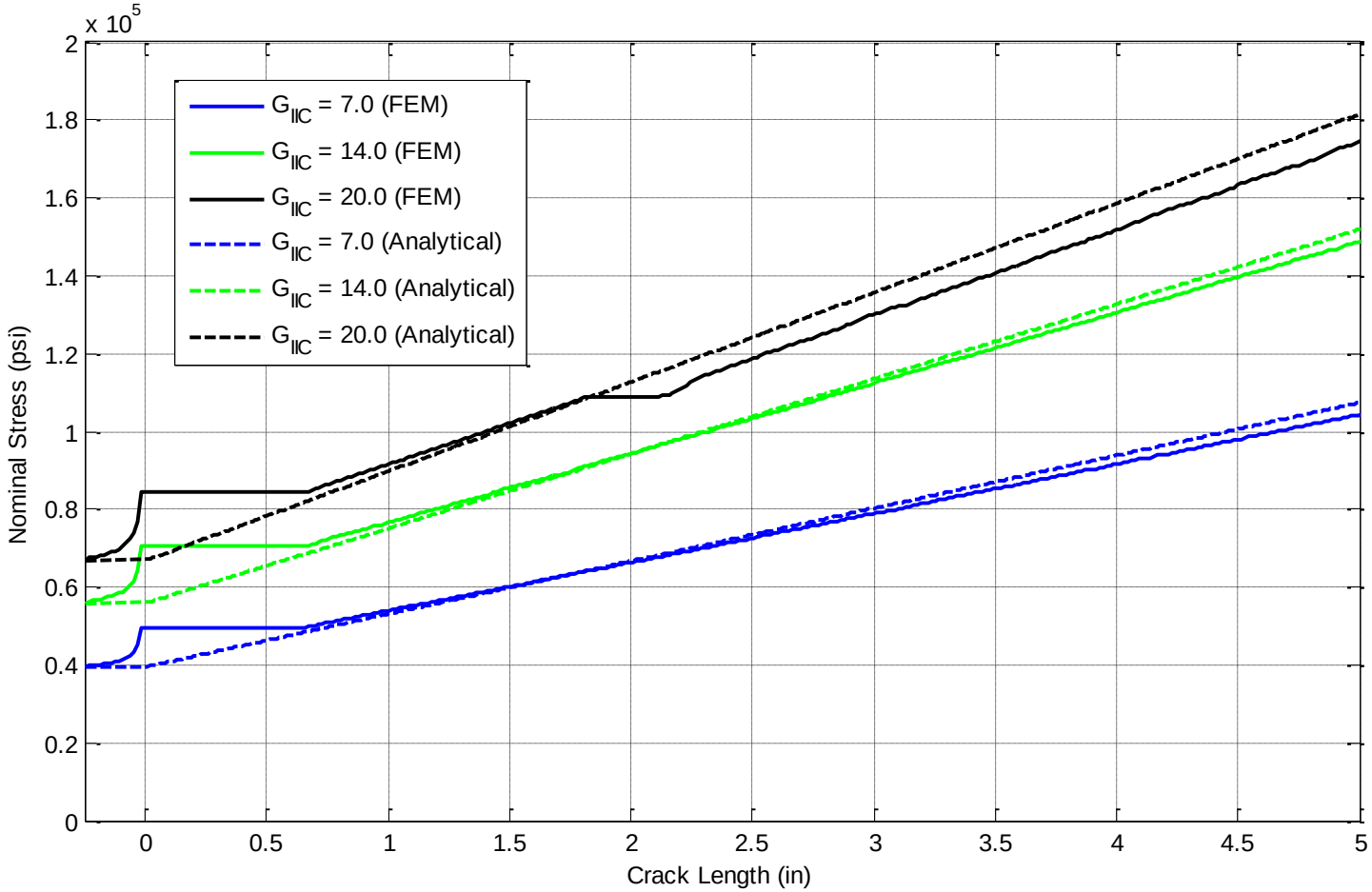

Figure 5.3: Comparison of Anaytical (plane-strain) and FEM crack growth simulations for G_{IIC} = 7.0, 14.0, 20.0 in-lb/in^2. Showing nominal stress versus crack length (fastener is at 0 in).

5.4 Parametric Analysis Using the Analytical Model

With the analytical model validated by the FEM, parametric analysis of the three-beam specimen can be conducted. The goal of the parametric analysis is to study the effect that changing various properties of the model (thickness, layup, fastener…) has on crack propagation behavior. All parametric analyses vary from a base configuration; the base configuration parameters are shown in Table 5.3.

The filled-hole tension failure is considered and is defined by $\varepsilon_{\mathrm{FHT}}$, which was measured during testing; it is assumed that this value is constant for all layups considered.

$$\varepsilon_{FHT} = 9460\ \mu\ in/in$$

Table 5.3: Base configuration for parametric analysis

Parameter	**Value**
Outer laminate layup	$[(0/45/90/-45)_3]_S$
Outer laminate thickness	0.18 in
Outer laminate E_x	7.424 Msi
Center laminate layup	$[(0/45/90/-45)_3]_S$
Center laminate thickness	0.18 in
Center laminate E_x	7.424 Msi
G_{IIC}	9.0 lb-in/in^2
Fastener diameter	0.25 in
Fastener material	Titanium
Fastener C	$4.64*10^{-6}$ in/lb

5.4.1 Variation of Laminate Stiffness

The stiffness of the outer and center laminates was varied, separately. The stiffness is varied by changing the layups only. The number of plies in each laminate is the same as the base configuration, so there is no change in laminate thickness. Three additional layups were considered for this parametric analysis; Table 5.4 summarizes the layup variations.

Table 5.4: Base configuration for parametric analysis

Layup	**E_x**	**Layup (percentage)**
$[90/45/0/-45/90/45/90/-45/90/45/0/-45]_S$	6.118 Msi	[17/50/33]
$[(0/45/90/-45)_3]_S$ (base configuration)	7.424 Msi	[25/50/25]
$[0/45/90/-45/0/45/0/-45/0/45/90/-45]_S$	8.683 Msi	[33/50/17]
$[(0/45/0/-45/0/90)_2]_S$	11.12 Msi	[50/33/17]

Figure 5.4 shows the effect of increasing the outer laminate layup/stiffness from the base configuration. An increase in outer laminate stiffness causes less load transfer to the center laminate at the crack tip, which results in an increase in crack propagation load and increased crack propagation stability; slope of the curves increases. This also means that the crack can propagate further before filled-hole tension failure, because the failure stress of the outer laminate is increased (assuming constant failure strain). Figure 5.5 shows the effect of increasing the center laminate layup/stiffness from the base configuration. An increase in the center laminate stiffness causes more load transfer from the outer laminate to the center laminate at the crack tip, which results in a decrease in crack propagation load and a decrease in crack propagation stability. The crack length at filled-hole tension failure is increased.

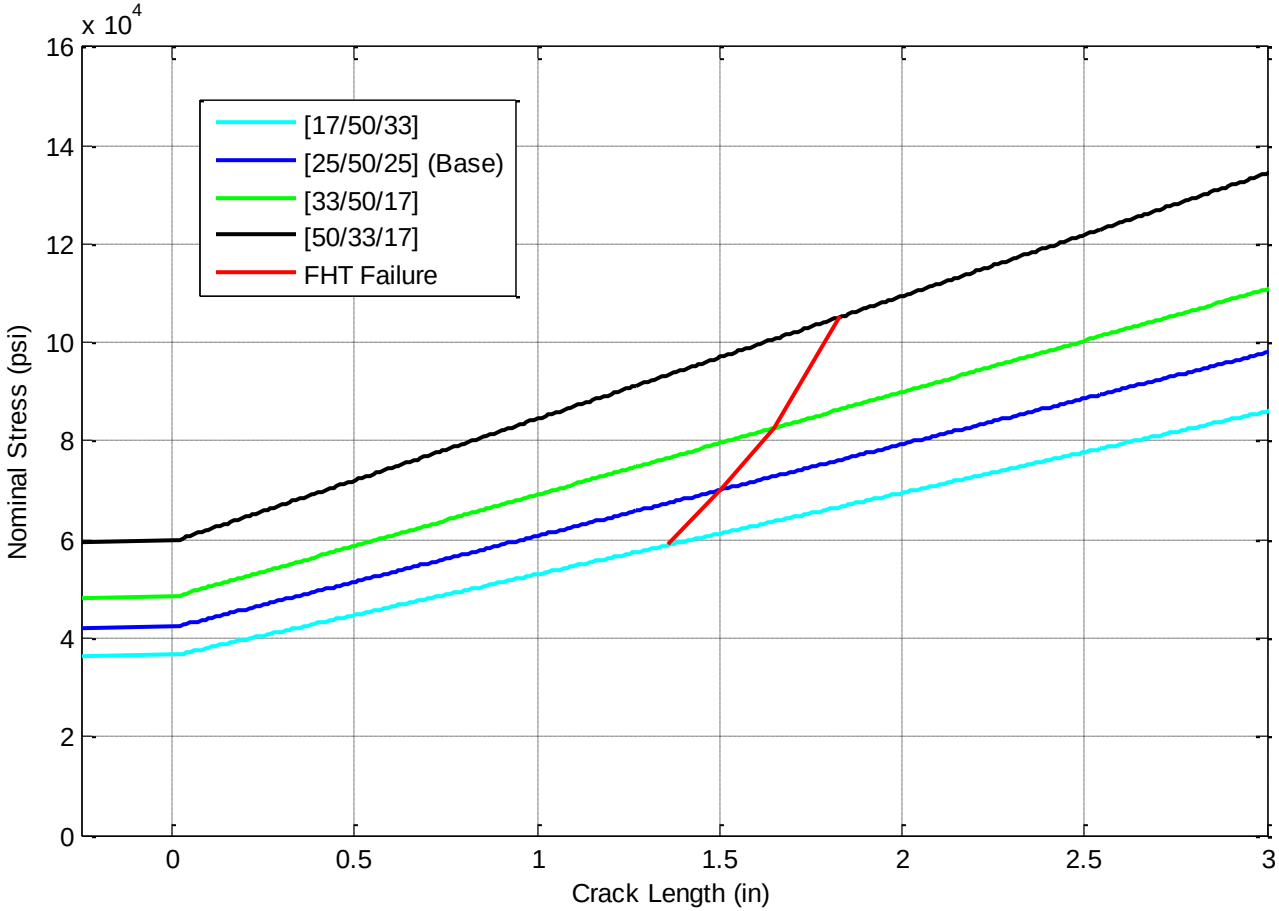

Figure 5.4: Parametric analysis of variation in outer laminate layup/stiffness. Nominal stress versus crack length.

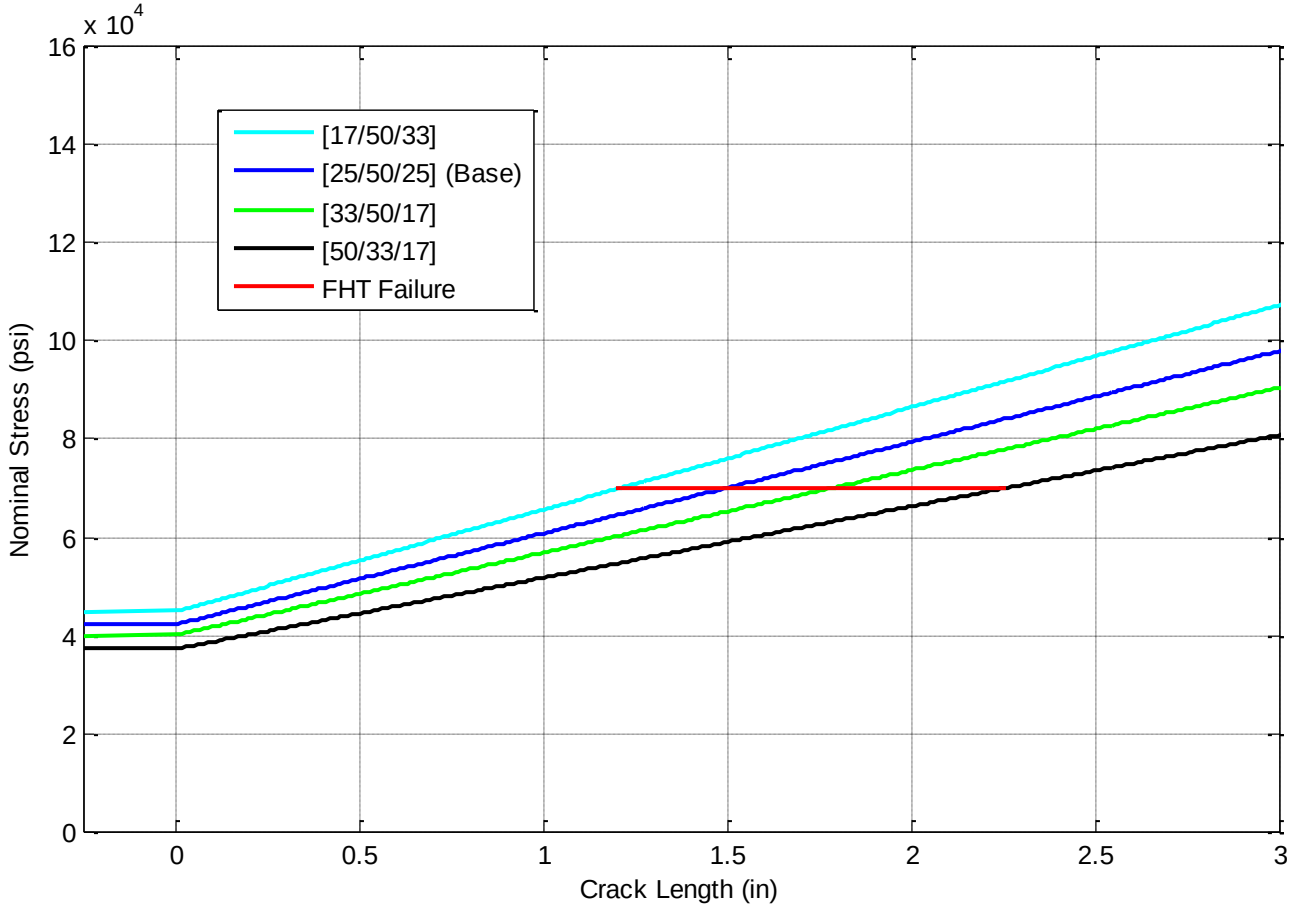

Figure 5.5: Parametric analysis of variation in center laminate layup/stiffness. Nominal stress versus crack length.

5.4.2 Variation of Laminate Thickness

The thickness of the outer and center laminates was varied, separately. The thickness is varied by increasing the number of plys, while maintaining the same quasi-isotropic base laminate layup. The effective modulus E_x remains the same for all layup configurations considered here. Three additional thicknesses were considered for this parametric analysis; Table 5.5 summarizes the layup variations.

Table 5.5: Laminate thickness variation descriptions

Layup	**Thickness**	**E_x**
$[(0/45/90/-45)_2]_S$	0.12 in	7.424 Msi
$[(0/45/90/-45)_3]_S$ (base configuration)	0.18 in	7.424 Msi
$[(0/45/90/-45)_4]_S$	0.24 in	7.424 Msi
$[(0/45/90/-45)_5]_S$	0.30 in	7.424 Msi

Figure 5.6 shows the effect of increasing the outer laminate thickness from the base configuration. An increase in outer laminate thickness causes less load to be transferred to the center laminate at the crack tip, which results in an increase in crack initiation load and an increase in crack propagation stability, greater slope of curves. This also means that the cracks propagate further past the fastener because the outer stress carried by the outer laminate is decreased from the base configuration. Figure 5.7 shows the effect of increasing the center laminate thickness from the base configuration. An increase in center laminate thickness causes more load transfer from the outer to center laminate at the crack tip, which results in a decrease in crack initiation load and a decrease in crack propagation stability; the slope of the curve decrease. Also, the cracks are able to propagate further past the fastener before filled-hole tension failure because the center laminate carries an increased load.

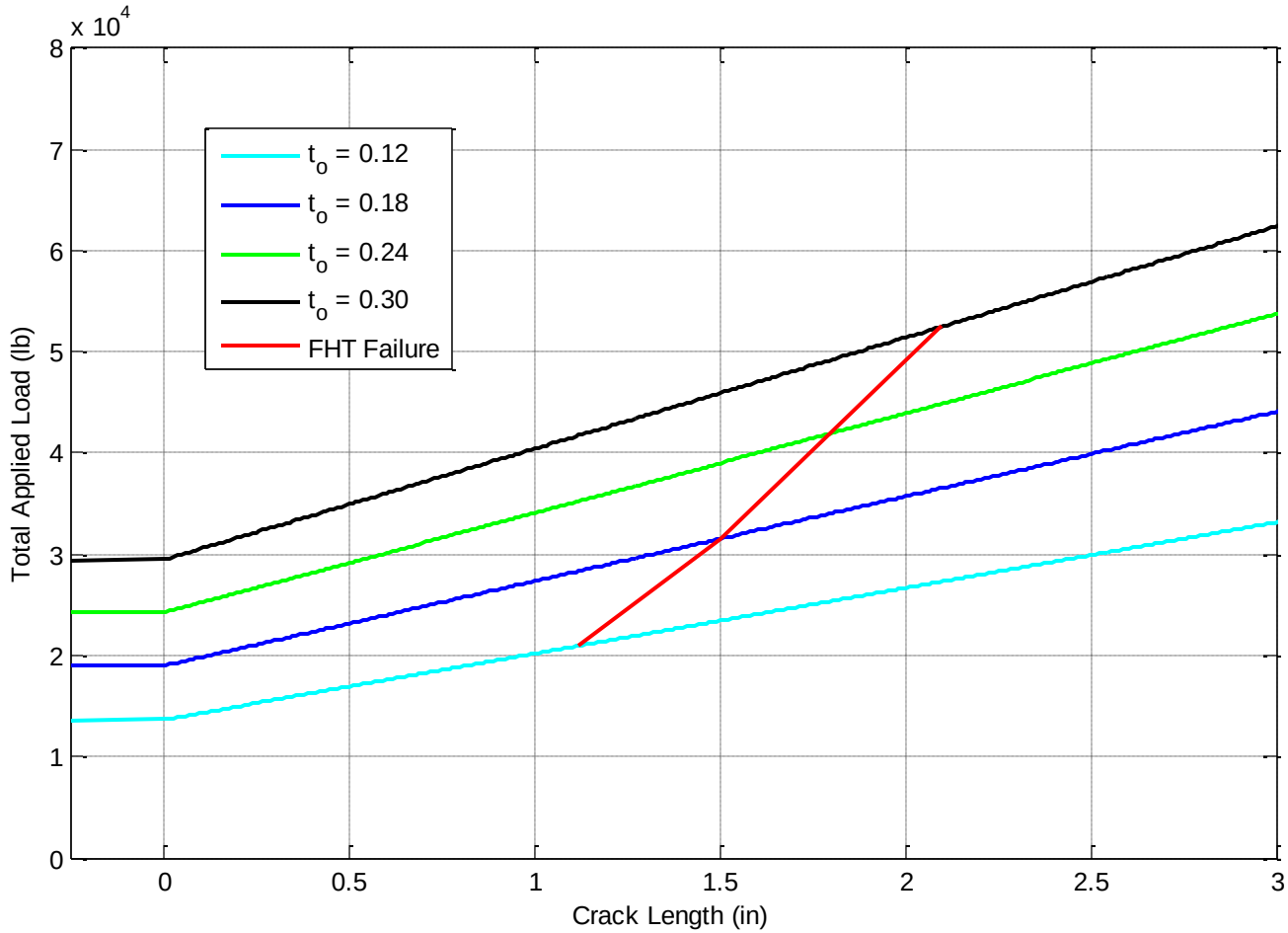

Figure 5.6: Parametric analysis of variation in outer laminate thickness. Total applied load versus crack length.

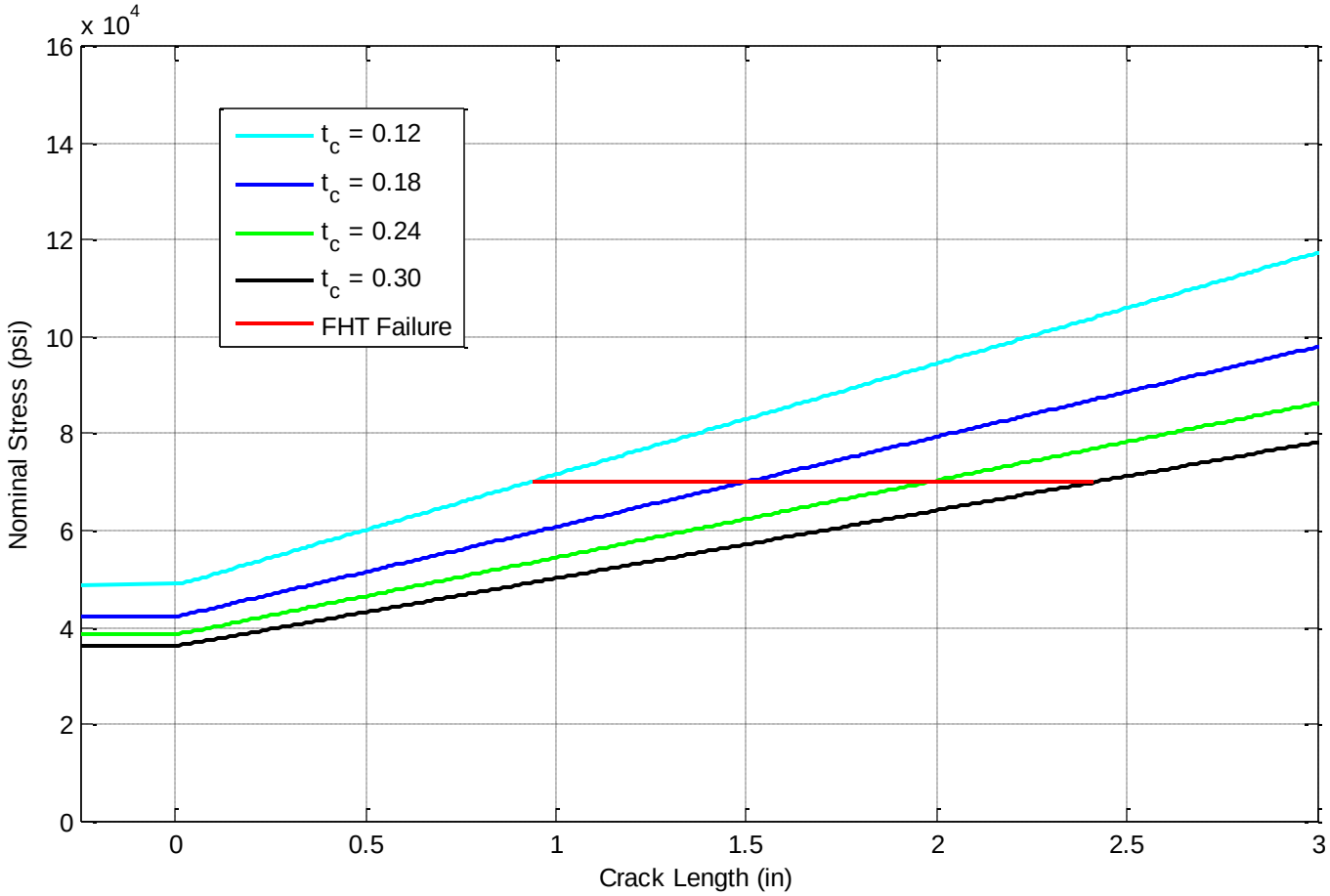

Figure 5.7: Parametric analysis of variation in center laminate thickness. Nominal stress versus crack length.

5.4.3 Variation of Fastener Compliance

The fastener compliance was varied by selecting different materials to represent the fastener. The diameter of the fastener was left at the base configuration value. The change in compliance caused by varying the diameter of the fastener was not considered here, because the size of the fastener hole with respect to the width of the specimen will result in a different filled-hole tension failure value. The new materials that were selected to represent the fastener are steel and aluminum. Fastener failure is considered. Table 5.6 summarizes the variation in fastener compliance, and shows typical shear strengths of each materal.

Table 5.6: Fastener Compliance Variation Values

Fastener Material	**Fastener Compliance**	**Fastener Shear Strength**
Aluminum	$5.24 * 10^{-6}$ in-lb/in^2	49.0 ksi
Titanium (Base configuration)	$4.64 * 10^{-6}$ in-lb/in^2	79.8 ksi
Steel	$3.32 * 10^{-6}$ in-lb/in^2	60.5 ksi

Figure 5.8 shows the effect of varying the fastener compliance from the base configuration. From the plot it can be seen that the crack initiation load is independent of fastener compliance; this is because the fastener is not carrying any load when the cracks initiate. A decrease in fastener compliance, equivalently an increase in fastener stiffness, results in more stable crack propagation. The reason for this is that the more stiffness the fastener has, the more load the fastener transfers from the outer laminate to the center laminate, which reduces the load transfer at the crack tip. The failure of each fastener in shear is shown on the plot: aluminum fails almost immediately after crack initiation, steel fails before filled-hole tension failure, and titanium does not fail.

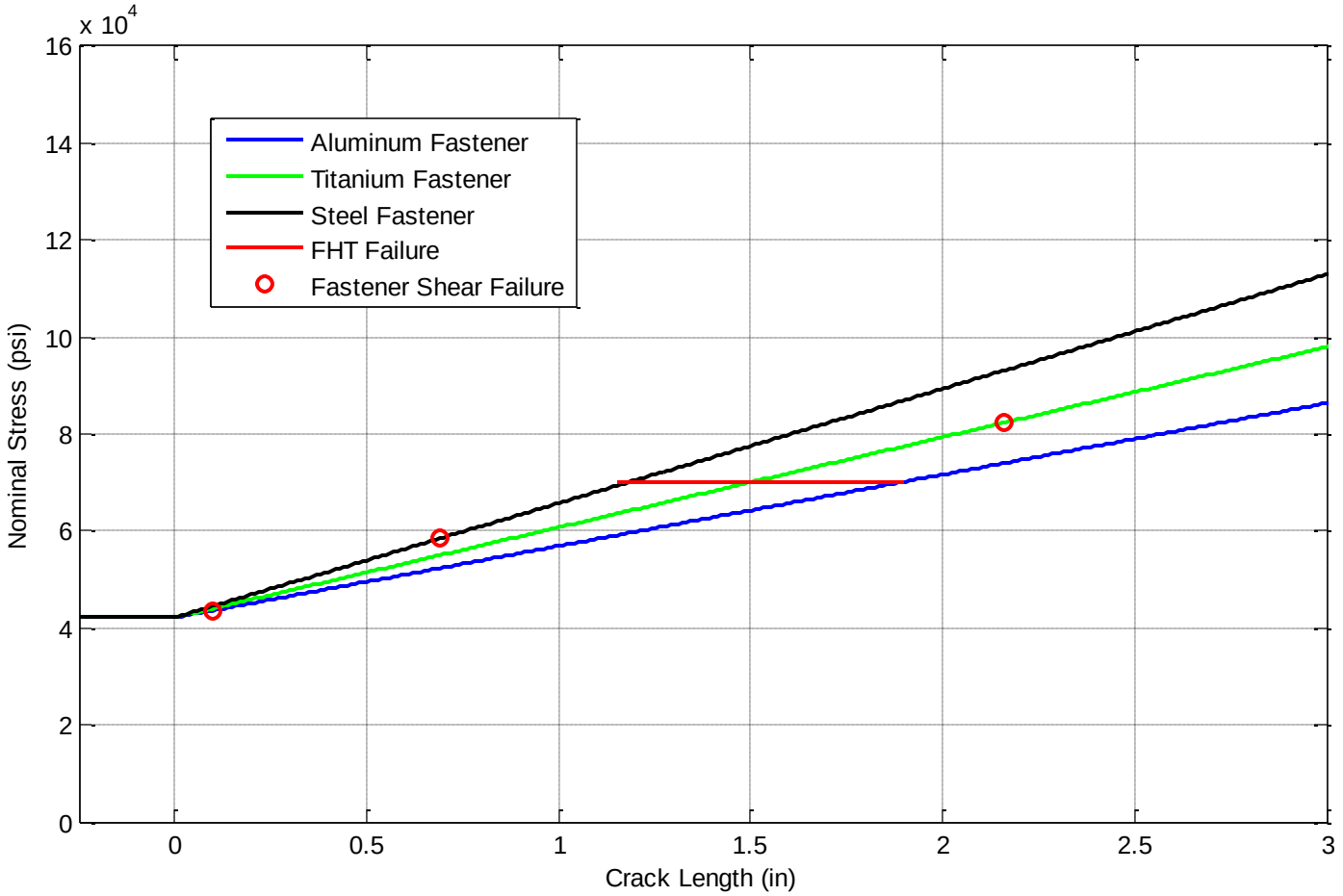

Figure 5.8: Parametric analysis of variation in fastener compliance. Nominal stress versus crack length.

5.4.4 Variation of Critical Strain Energy Release Rate G_{IIC}

The strength of the bond between the laminates was varied by selecting different values of G_{IIC} for the bond line. The values that were selected for this parametric study were from the values that were measured from the actual test specimens. The reason for this was to study the theoretical behavior of the specimens that were tested based on the current analytical method. The G_{IIC} values for the actual test specimens were calculated from Equation 5.23, which is re-stated below, using the average measured crack propagation loads, P_C, that were obtained from testing. Figure 5.9 shows the analytical predictions of the different bond interface configurations that were tested; the secondary bond [0/90] fabric interface and secondary bond 0/0 interface specimens had the same crack initiation loads, so they are analyzed as a single configuration.

$$G_{IIC} = P_C^2 \left[\frac{-2\left(aA_cE_c + 2aA_oE_o + A_cA_oC_fE_cE_o\right)^2}{8A_i\left(aA_cE_c + 2aA_oE_o + A_cA_oC_fE_cE_o\right)^2E_i} + \cdots \right.$$

$$\left. \cdots + \frac{A_i(2a^2A_cE_c + A_o\left(2a + A_cC_fE_c\right)^2E_o)E_i}{8A_i\left(aA_cE_c + 2aA_oE_o + A_cA_oC_fE_cE_o\right)^2E_i} \right]$$

Table 5.7: Predicted bond strengths of all test coupon configuration.

Bond Interface Description	**Average P_C**	**Measured G_{IIC}**
Secondary bond [0/90] fabric interface and 0/0 interface	36.3 kip	31.5 in-lb/in^2
Co-cured 0/0 interface	20.3 kip	11.1 in-lb/in^2
Co-cured ±45 interface	27.9 kip	18.9 in-lb/in^2
Modified Bond 1	31.1 kip	23.5 in-lb/in^2
Modified Bond 2	42.2 kip	43.3 in-lb/in^2

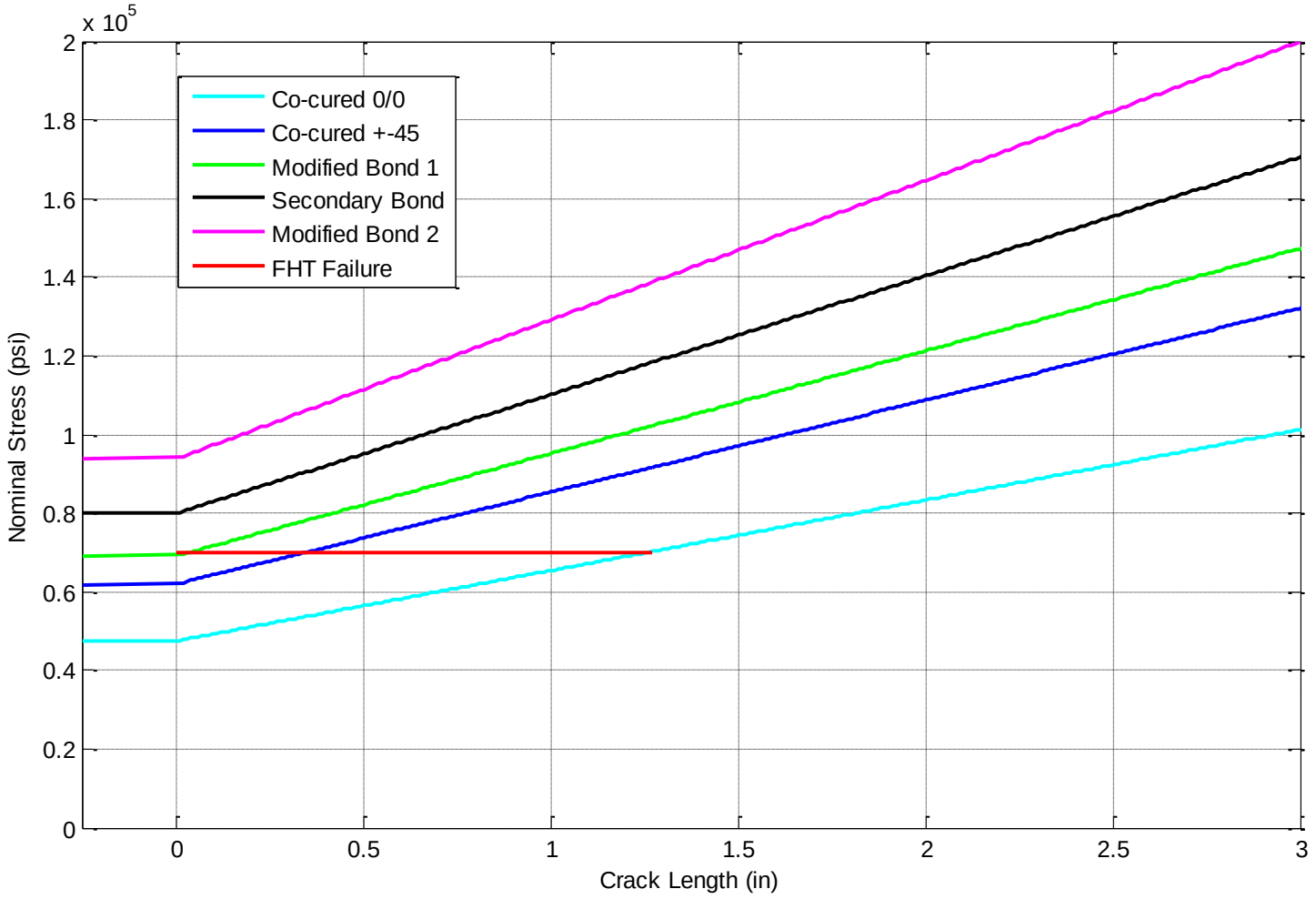

Figure 5.9: Analytical predictions of test specimens using predicted G_{IIC}.

Figure 5.9 shows the analytical predictions of the different bond interface configurations that were tested. The analytical predictions are based on the material properties, loads, and strains that were measured during testing. The analytical predictions reasonably reflect how the actual tests occurred. Testing and inspection of both types of co-cured specimens showed that the cracks reached approximately 0.5-1.125 in past the fastener, which is on the same order of what the analysis predicts. For all other specimens where the crack initiation load was nearly equal to or greater than the filled-hole tension failure load, the analytical model cannot be reasonably compared, because crack initiation and failure occurred almost simultaneously.

There are some physical behaviors that the analytical model does not take into account; these limit the analysis capabilities to accurately predict the pure Mode II crack propagation behavior of the specimen configuration. The analytical model does not include the clamping force from fasteners. As a result of this, the friction that occurs at the bond interface is not modeled. The friction force acts to stabilize the crack in the region near the fastener. The analytical model does not consider a crack front, it considers the location of a crack as a single point, but the crack changes its shape drastically as it propagates around the fastener. Despite the analytical models' limitations, it does provide a good tool for studying the general behavior of the pure Mode II crack propagation in the test specimen and similar structures. The analytical model also provides good insight into how changing structural parameters will affect the growth and arrestment of cracks.

Chapter 6

SUMMARY AND CONCLUSIONS

The capability of a fastener to arrest and stabilize pure Mode II crack propagation in composite structures has been investigated both experimentally and analytically. A novel composite three-beam axially loaded test specimen was designed to provide pure Mode II interlaminar failure. A FEM simulation of the proposed specimen verified that crack propagation was pure Mode II.

The Boeing Co. manufactured a variety of specimens, all with quasi-isotropic laminates and of the same geometry, but differing in bonding technique and plies at the crack interface. Testing of the specimens showed that if the fracture toughness of the bond between beams is too high, then the crack initiation load is higher than the filled-hole tension failure load of the outer laminates, which limits the data available to study the crack arrestment capabilities of the fastener. This occurred in the secondary bond, ±45 co-cured, and modified bond 2 specimens. Even though this occurred, post failure C-scan and A-scan inspections showed that the presence of the fastener did in fact prevent cracks from propagating by, while the absence of a fastener allowed the crack to travel past the fastener hole. For the specimens whose crack initiation loads were lower than the filled-hole tension failure load, the tests revealed that cracks propagated to the location of the fastener, or in some cases well beyond the fastener, where they were stabilized and arrested as the load in the specimen continued to increase.

Testing also showed that the crack propagation behavior of the specimens depended on the plies used at the crack interface. All 0/0 interfaces, co-cured and secondary bond, showed cohesive crack propagation. While the secondary bond [0/90] fabric interface and ±45 co-cured interface both failed non-cohesively; the cracks jumped a couple of plies into the outer laminates and continued to propagate at a 90/45 interface. The significance of this is that the cross-sectional area of the outer laminates is reduced, therefore reducing filled-hole

tensile failure load of the specimen. Crack propagation of the modified bond specimens was cohesive, but the details of how the bonds were modified were not disclosed by the manufacturer.

An analytical model based on an idealization of the specimen was developed. From the analytical mode, a closed-form solution that predicts the critical load at which a crack propagates was derived directly from the definition of SERR. The analytical model was verified with FEM and showed very good comparison. The solution was used to simulate crack arrestment capabilities of the fastener for variations in specimen parameters. The following parameters were varied: laminate layup (stiffness), laminate thickness, fastener compliance, and G_{IIC} of the bond. The analytical model showed that crack stabilization is improved by increasing outer laminate stiffness, outer laminate thickness, fastener compliance, and bond strength.

Further experimental work is necessary to fully study the crack arrestment capabilities of the fastener using the three-beam specimen. It is suggested that the experimental results and analytical model be used to aid in the design a specimen that will allow maximum crack propagation before ultimate failure of the specimen. Additionally, a more detailed study into the load transferred by the fastener would be very useful for further validation of the analytical model. Further improvements of the analytical model could be made by including the effect of fastener clamping and friction.

LIST OF REFERENCES

1. Jen, M. H. R. and Lin W. H., "Innovative Fracture Tests of Single-Lapped Bolted and Bonded Composite Joints," *Journal of Reinforced Plastics and Composites*, Vol. 19 No. 18, 2000, pp. 1444-1473.
2. Jen, M-H. R. and Lin W. H., "Strength of Bolted and Bonded Single-Lapped Composite Joints in Tension," *Journal of Composite Materials*, Vol. 33, 1999, pp. 640-666.
3. Lee, Y. H., Lim, D. W., Choi, J. H., Kweon, J. H., and Yoon, M. K., "Failure Load Evaluation and Prediction of Hybrid Composite Double Lap Joints," *Composite Structures*, Vol. 92, 2010, pp. 2916-2926.
4. ASTM Standard D6671/D6671M-06, "Standard Test Method for Mixed Mode I-Mode II Interlaminar Fracture Toughness of Unidirectional Fiber Reinforced Polymer Matrix Composites," ASTM International, West Conshohoken, Pennsylvania, 2006, DOI: 10.1520/D6671_D6671M-06.
5. Todo, M., Nakamura, T., and Takahashi, K., "Mode II Interlaminar Fracture Behavior of Fiber Reinforced Polyamide Composites under Static and Dynamic Loading Conditions," *Journal of Reinforced Plastics and Composites*, Vol. 18, pp.1415-1427.
6. Carlsson, L. A., Gillespie, J. W., and Pipes, R. B. "On the Analysis and Design of the End Notched Flexure (ENF) Specimen for Mode II Testing," *Journal of Composite Materials*, Vol. 20, 1986, pp 594-604.
7. Tate, M. B., and Rosenfeld, S. J., "Preliminary Investigation of Loads Carried by Individual Bolts in Bolted Joints," Technical Note No. 1051, National Advisory Committee of Aeronautics, 1984.
8. Huth, H., "Influence of Fastener Flexibility on the Prediction of Load Transfer and Fatigue Life for Multiple-Row Joints," *Fatigue in Mechanically Fastened Composite and Metallic Joints, ASTM STP 927*, John M. Potter, Ed., American Society for Testing and Material, Philadelphia, 1986, pp. 221-250.
9. Krueger, R., "The Virtual Crack Closure Technique: History, Approach and Applications," NASA/CR-2002-211628, ICASE Report No. 2002-10, April 2002.

10. Mabson, G., DeoBald, L., and Dopker B., "Fracture Interface Elements for the Implementation of the Virtual Crack Closure Technique," *AIAA-2007-2376, 48th AIAA/ASME/ASCE/AHS/ASC Structures, Structural Dynamics, and Materials Conference,* Honolulu, Hawaii, Apr. 23-26, 2007.
11. Wang, J., Qiao, P., "Fracture Analysis of Shear Deformable Bi-Material Interface," *Journal of Engineering Mechanics,* Vol. 132, 2006, pp. 306-316.